Multibody Syst Dyn (2010) 24: 413–439
DOI 10.1007/s11044-010-9202-2

Dynamic modeling and stability analysis of a power-generating tumbleweed rover

James R. Forbes · Timothy D. Barfoot · Christopher J. Damaren

Received: 27 October 2008 / Accepted: 9 March 2010 / Published online: 13 May 2010

Abstract This paper introduces a novel tumbleweed rover design that employs a pendulum–generator system to harvest electrical power from the wind. First, the dynamics of this multibody system are developed, including the internal pendulum dynamics, resistance (damping) provided by the electrical generators, external wind force, and rolling constraints between the sphere and the ground. Second, the stability of the system (without wind) is studied and it is shown that it is stable in the sense of Lyapunov. Finally, simulation results are provided that verify the system will roll stably downwind while generating power.

Keywords Multibody dynamics · Tumbleweed rover · Pendulum · Planetary exploration

1 Introduction

The twin Mars Exploration Rovers (MER), Spirit, and Opportunity, have been an overwhelming success. These two rovers, which landed in early 2004, have vastly exceeded their 90-day life expectancy. As a result of using these ground-breaking tools, humankind has learned more about the geology, mineralogy, and meteorology of Mars in the last 5 years than in all of previous history. Despite these monumental achievements, it has taken an average of 4 months for a MER rover to drive 1 kilometer. To truly understand scientific properties on a planetary scale, it is desirable to acquire scientific data across as large an area as possible.

One approach to achieving large-scale exploration is to continue to advance the on-board autonomy techniques that allow conventional six-wheeled rovers to make decisions on their

J.R. Forbes · T.D. Barfoot (✉) · C.J. Damaren
University of Toronto Institute for Aerospace Studies, 4925 Dufferin Street, Toronto, Ontario M3H 5T6, Canada
e-mail: barfoot@utias.utoronto.ca

J.R. Forbes
e-mail: forbes@utias.utoronto.ca

C.J. Damaren
e-mail: damaren@utias.utoronto.ca

own. The MERs showed that autonomous operations could increase the amount of time spent carrying out science [1], as compared to the 1997 Sojourner rover (which had very limited autonomy). In particular, the MERs employed stereo cameras to help detect and avoid rocks and hazards when driving between scientific sampling locations. However, this capability has only been enabled for 25% of the distance traveled by the two rovers, in large part because it is overly conservative when deciding what terrain is safe. For the other 75% of the distance traveled, human operators on Earth have laboriously uploaded commands based on images downloaded from Mars during the infrequent communication windows.

Another approach to covering larger distances is to reduce the dependence on solar power, as this limits the operations that can occur within a given sol. The next six-wheeled rover, Mars Science Laboratory (MSL), will be approximately twice as large as the MERs, will employ a nuclear power source, and will start its mission with the latest autonomy capabilities afforded to the MERs. These advantages together will potentially increase the distance covered by MSL as compared to the MERs. However, this will likely not result in a rover that can travel hundreds, even thousands of kilometers.

A more radical approach to large-scale exploration is to completely change the design of the rover. In this paper, we consider a wind-powered *tumbleweed rover*. The idea is simple; an inflated ball is blown by the Martian winds, much like a tumbleweed is blown across a terrestrial desert. In its most basic form, as the rover is blown and rolls along with the wind, it collects data such as temperature, pressure and surrounding light intensity and transmits it back to Earth. The impetus to use a tumbleweed rover is its simplicity; a rover that uses the surrounding environment as propulsion requires less equipment such as motors, power, motion control, etc. In turn, with the mass reduction of the rover, more science experiments can be added, creating missions with more objectives, which translates to higher scientific yield. Field trials on Earth with tumbleweed prototypes have shown the ability for these systems to travel over 100 kilometers fully autonomously [2].

Tumbleweed rovers have been studied by a handful of organizations in the past including the NASA Jet Propulsion Lab [3] and NASA Langley Research Center [4]. In this paper, we introduce and study a novel tumbleweed rover design that enjoys a number of potential advantages over its competitors:

1. It employs an internal pendulum-generator system to produce electrical power as a result of being blown by the wind. This removes the need for solar panels while providing abundant power for the avionics and payload.
2. By varying the amount of electrical power harvested, this provides a means to regulate the speed of the rover.
3. By storing the electrical power generated in times of high winds in a battery (likely located in the pendulum for ballast), the rover can reverse the flow of electricity and use the generators as motors to self-propel in times of low winds.
4. With the pendulum laterally fixed, the rover is naturally stable and will roll downwind about its preferred axis. This provides a stable platform to potentially carry camera systems or other sensors with pointing requirements.
5. With the pendulum laterally controlled, the rover is able to steer itself both in the presence and absence of wind. This opens the possibility for hazard avoidance and visiting specific sites of interest.

One conceptual design of our tumbleweed rover is shown in Fig. 1.

The purpose of this paper is to present a first-principles approach to three-dimensional dynamic modeling of our tumbleweed rover concept including such effects as the internal

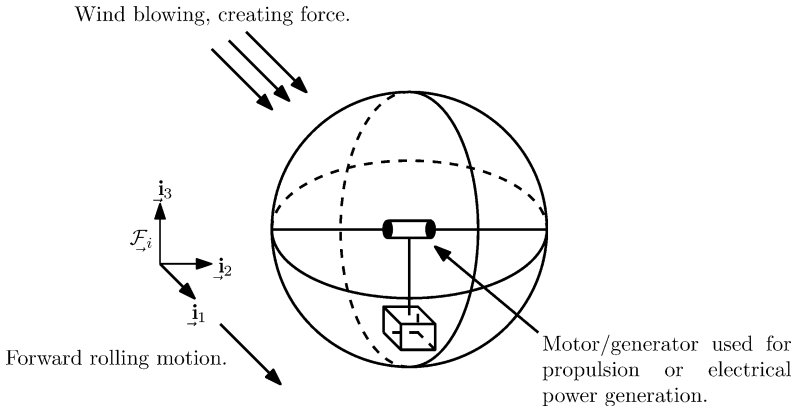

Fig. 1 One possible implementation of the tumbleweed rover discussed in this paper

pendulum dynamics, resistance (damping) provided by the electrical generators, external wind force, and rolling constraints between the sphere and the ground. This is an important step as it allows us to prove out the basic stability of our concept and to select key design parameters (e.g., masses, lengths) before building a prototype. To this end, we use our model to consider the case in which the payload pendulum is laterally fixed and prove the tumbleweed is naturally stable. We validate these findings through dynamic simulations. We begin with a brief discussion of related work.

2 Related work

Tumbleweed rovers have been proposed for various Mars missions including to study gully formations in such locations as Dao Vallis [5–7] and to measure small-scale magnetic anomalies in the Southern Highlands [8]. The commonality between the various concepts is that they all propose to harness the wind to propel a large round vehicle long distances across the surface. However, there is quite a bit of variability in the concepts that have been proposed.

NASA Jet Propulsion Laboratory has focused on a large inflatable sphere design with a central cylindrical payload [3, 9]. This design has been field tested in Greenland [2], Antarctica, and sites within the United States [10]. The design has performed extremely well, allowing measurements such as temperature and pressure to be gathered over distances greater than 100 kilometers. The inflatable design is promising in that it offers a built-in deployment mechanism and possibly also a landing mechanism (i.e., it serves as its own airbag). One downside is that the inflatable nature of the design means that it is subject to puncturing and requires periodic pumping to maintain internal pressure. The current JPL design does not attempt to provide a means to steer the ball, but experiments have shown that it rotates about the preferred payload axis in high winds. There is also no way to slow down the vehicle other than to deflate. Most of the field deployments to date have used a battery to provide electrical power to the avionics and payload. There have also been some investigations into using flexible solar panels affixed to the exterior of the inflatable ball [10]. This would certainly have negative implications for deployment/landing and it would be difficult to protect the solar arrays during movement. The design we study in this paper is related to the JPL design in that it would most likely make use of an inflatable outer shell.

NASA Langley Research Center (with collaborators from Orbital Research Inc., North Carolina State University, and Case Western Reserve University) has been developing tumbleweed concepts in parallel to the JPL work [4]. Their designs are partially inspired by the Russian thistle [11], a natural tumbleweed. Several concepts have been investigated including Wedges, Box-Kite, Dandelion, Eggbeater Dandelion, and Tumble-Cup [12]. The baseline design selected for further testing was the Box-Kite [13, 14]. Various deployment and solar array concepts were examined [15], with a gimbaled central payload selected for the Box-Kite with an upward-looking solar panel. The Box-Kite design is appealing in that it has a higher drag coefficient than a solid ball, is not susceptible to punctures, and does not require continual pumping to maintain pressure. However, the design does not offer a large payload area and deployment could be complicated. The frame to support the sails could also become lodged on rocks. To slow the vehicle down either a set of offset masses could be used or the sails could be lowered [6], but both these methods require additional mechanisms thereby increasing complexity.

The tumbleweed rover we study in this paper is different from the JPL inflatable tumbleweed and Langley Box-Kite in several important ways: (i) we generate power internally using the pendulum–generator concept, (ii) we regulate the speed of the vehicle by removing energy from the system through our power generation concept, (iii) the presence of the pendulum offers orientation stability at low speeds and also the ability to steer, and (iv) we have a means to propel the vehicle when the winds are low.

The most similar concept to our design is the steered tumbleweed, called Thistle, developed at the Helsinki University of Technology for the European Space Agency [16]. This rover is blown by the wind, and has a pendulum that enables it to steer and propel itself when winds are low. However, it does not have the capability to harvest power from the wind and as a by-product regulate speed. Moreover, driving tests showed the motion of the vehicle to be "quite clumsy and somewhat chaotic". This provides important motivation for the dynamic modeling and stability analysis in this paper. We seek to prove out our concept and select appropriate design parameters through simulation, prior to building a prototype.

In terms of dynamic modeling of tumbleweed rovers, there has been some prior work. Both [4] and [11] conduct two-dimensional quasi-static and dynamic analyses of tumbleweeds (with no pendulum) to draw conclusions about obstacle negotiation and slope climbing capabilities. Rock distribution models are used to predict the distance a tumbleweed will be able to travel before encountering a rock too large to surmount. In [10], there is some discussion of dynamic modeling, particularly of the aerodynamics of the tumbleweed scenario, but little is presented in the way of a dynamic model that could be used for three-dimensional simulation and stability analysis. In [17], a detailed three-dimensional dynamic model is presented that includes bouncing effects. This model is clearly targeted at the Langley Box-Kite tumbleweed design; it is not capable of simulating an internal pendulum with electrical resistance or rolling constraints between the sphere and the ground. In [6] a commercial modeling package is used to conduct dynamic simulations, but this does not allow for any analytical stability analyses to be carried out.

In summary, there has been little discussion of wind-driven tumbleweeds that incorporate a pendulum and none that have generated power by this means. As such, there has also been little presented in terms of dynamic modeling of this tumbleweed design. For a more detailed review of tumbleweed designs, see [18] and for a historical perspective on ball-shaped robots see [16].

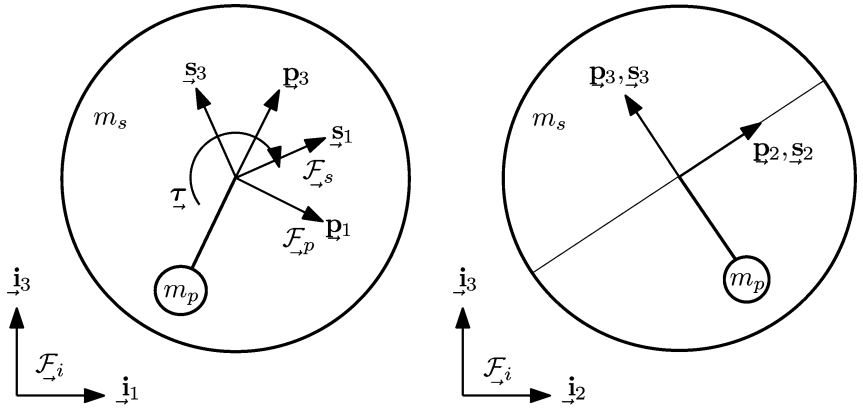

(a) Side view. (b) Front view.

Fig. 2 Tumbleweed rover with payload pendulum

3 Model setup

Consider the tumbleweed rover depicted in Fig. 2. A reference frame, $\vec{\mathcal{F}}_s$, is fixed to the sphere[1] with its origin at the center. The nominal rotation of the sphere is about the $\vec{\mathbf{s}}_2$-axis. Normally, the $\vec{\mathbf{s}}_2$-axis of the sphere frame is parallel to the $\vec{\mathbf{i}}_1$–$\vec{\mathbf{i}}_2$ plane (which represents the nominal ground plane) of the inertial frame, $\vec{\mathcal{F}}_i$. The sphere has a 'central rod' passing through it along the $\vec{\mathbf{s}}_2$-axis. Hung from the center of the central rod is a mass, called the 'payload'. In practice, the payload could include avionics, batteries, and scientific instruments. The rod connecting the payload to the central rod will be called the 'pendulum'. We attach a third reference frame, $\vec{\mathcal{F}}_p$, to the payload (and pendulum), whose origin is again at the center of the sphere. In the case that the pendulum is fixed laterally, $\vec{\mathbf{s}}_2$ and $\vec{\mathbf{p}}_2$ will be coincident; in the case that the pendulum is free to move laterally, this will no longer be true.

The main feature of this rover design is the presence of mechanical resistance, in the form of a torque about the $\vec{\mathbf{s}}_2$-axis created by an electrical generator, between the pendulum and the central rod. As the sphere is blown by the wind, the generator will resist rotational motion, causing the payload to rise up (rotate about the $\vec{\mathbf{s}}_2$-axis), thus regulating the speed of the sphere as it rolls. If the mechanical resistance created via power generation is controlled, the velocity of the sphere can also be controlled. Therefore, not only can the velocity of the sphere be controlled, but in doing so power is generated.

4 Notation

In order to concisely describe the dynamic equations of motion, a standard notation set will be defined.

4.1 General

We elect to use Vectrix notation, which is described in [19]. Briefly, we have the following:

[1] We will use the terminology 'sphere' and 'tumbleweed' interchangeably.

$\underset{\rightarrow}{\mathbf{v}}$	a vector, which is independent of reference frame
$\underset{\rightarrow}{\mathcal{F}}_a = [\underset{\rightarrow}{\mathbf{a}}_1 \ \underset{\rightarrow}{\mathbf{a}}_2 \ \underset{\rightarrow}{\mathbf{a}}_3]^{\mathrm{T}}$	a vectrix of basis vectors forming a reference frame
$\mathbf{v}_a = [v_1 \ v_2 \ v_3]^{\mathrm{T}}$	a column containing the coordinates of a vector with respect to the basis vectors in a particular reference frame

Using the above definitions, we have that

$$\underset{\rightarrow}{\mathbf{v}} = \underset{\rightarrow a}{\mathcal{F}}^{\mathrm{T}} \mathbf{v}_a = v_1 \underset{\rightarrow}{\mathbf{a}}_1 + v_2 \underset{\rightarrow}{\mathbf{a}}_2 + v_3 \underset{\rightarrow}{\mathbf{a}}_3.$$

In Vectrix notation, the cross product of two vectors $\underset{\rightarrow}{\mathbf{v}}$ and $\underset{\rightarrow}{\mathbf{u}}$, where $\mathbf{v}_a = [v_1 \ v_2 \ v_3]^{\mathrm{T}}$ and $\mathbf{u}_a = [u_1 \ u_2 \ u_3]^{\mathrm{T}}$, is expressed using a 3×3 skew-symmetric matrix

$$\underset{\rightarrow}{\mathbf{v}} \times \underset{\rightarrow}{\mathbf{u}} = \underset{\rightarrow a}{\mathcal{F}}^{\mathrm{T}} \begin{bmatrix} 0 & -v_3 & v_2 \\ v_3 & 0 & -v_1 \\ -v_2 & v_1 & 0 \end{bmatrix} \begin{bmatrix} u_1 \\ u_2 \\ u_3 \end{bmatrix} = \underset{\rightarrow a}{\mathcal{F}}^{\mathrm{T}} \mathbf{v}_a^{\times} \mathbf{u}_a$$

where

$$\mathbf{v}_a^{\times} := \begin{bmatrix} 0 & -v_3 & v_2 \\ v_3 & 0 & -v_1 \\ -v_2 & v_1 & 0 \end{bmatrix}.$$

4.2 Physical parameters

The following parameters describe the physical characteristics of the dynamic system and its surrounding environment:

g	gravitational acceleration
r	radius of sphere
m_{s}	mass of sphere
$\mathbf{J}_{\mathrm{s}}$	second moment of mass of sphere, expressed in $\underset{\rightarrow}{\mathcal{F}}_{\mathrm{s}}$
b_{r}	damping coefficient associated with rolling friction
b_{s}	damping coefficient associated with spin friction
m_{p}	mass of pendulum rod and payload
$\mathbf{J}_{\mathrm{p}}$	second moment of mass of pendulum rod and payload combined, expressed in $\underset{\rightarrow}{\mathcal{F}}_{\mathrm{p}}$
$\mathbf{c}_{\mathrm{p}}$	first moment of mass of pendulum rod and payload combined, expressed in $\underset{\rightarrow}{\mathcal{F}}_{\mathrm{p}}$
l	length of pendulum
b_{p}	damping coefficient associated with payload as a result of on-board power generation

4.3 Miscellaneous

It will also be useful to define $\mathbf{x} := [1 \ 0 \ 0]^{\mathrm{T}}$, $\mathbf{y} := [0 \ 1 \ 0]^{\mathrm{T}}$ and $\mathbf{z} := [0 \ 0 \ 1]^{\mathrm{T}}$.

5 Kinematic relations and constraints

5.1 Angular and translational velocities

To describe the ball and pendulum motions, we require their respective angular velocities. The angular velocity of the sphere with respect to the inertial frame is $\boldsymbol{\omega}_{\mathrm{s}}^{\mathrm{si}}$ where the superscript denotes 'sphere frame with respect to inertial frame' and the subscript denotes

'expressed in frame $\vec{\mathcal{F}}_{\mathrm{s}}$'. The angular velocity of the payload with respect to the inertial frame is $\boldsymbol{\omega}_{\mathrm{p}}^{\mathrm{pi}}$ where the superscript denotes 'payload frame with respect to inertial frame' and the subscript denotes 'in frame $\vec{\mathcal{F}}_{\mathrm{p}}$'. The orientations of the frames $\vec{\mathcal{F}}_{\mathrm{s}}$ and $\vec{\mathcal{F}}_{\mathrm{p}}$ with respect to $\vec{\mathcal{F}}_{\mathrm{i}}$ are described by the rotation matrices $\mathbf{C}_{\mathrm{si}}$ and $\mathbf{C}_{\mathrm{pi}}$, respectively.

In general, the orientation of each body can be described by any general Euler angle sequence (e.g., a 3-1-2 sequence). The Euler angles defining the rotation matrix $\mathbf{C}_{\mathrm{si}}$ are denoted $\boldsymbol{\theta}^{\mathrm{si}}$, and those defining the rotation matrix $\mathbf{C}_{\mathrm{pi}}$ are denoted $\boldsymbol{\theta}^{\mathrm{pi}}$. We will often make use of the following relationships between Euler angle rates and angular velocities

$$\boldsymbol{\omega}_{\mathrm{s}}^{\mathrm{si}} = \mathbf{S}_{\mathrm{s}}^{\mathrm{si}} \dot{\boldsymbol{\theta}}^{\mathrm{si}}, \qquad \boldsymbol{\omega}_{\mathrm{s}}^{\mathrm{pi}} = \mathbf{S}_{\mathrm{p}}^{\mathrm{pi}} \dot{\boldsymbol{\theta}}^{\mathrm{pi}}$$

where $\mathbf{S}_{\mathrm{s}}^{\mathrm{si}}$ and $\mathbf{S}_{\mathrm{p}}^{\mathrm{pi}}$ are the appropriate mapping matrices between the Euler angle rates and the angular velocities [19]. Recall that $\boldsymbol{\omega}_{\mathrm{s}}^{\mathrm{si}}$ and $\boldsymbol{\omega}_{\mathrm{p}}^{\mathrm{pi}}$ are each expressed in terms of quasi-coordinate rates.[2]

5.2 System constraints

Non-holonomic constraints are those which are non-integrable. The tumbleweed rover system is constrained by two non-holonomic constraints: one related to the rolling motion, and the other related to the pendulum motion.

5.2.1 Rolling constraint

Consider the tumbleweed rover, as shown in Fig. 3, where the pendulum is not drawn. Assuming the sphere rolls without slipping, we can express the sphere's translational velocity in term of its angular velocity.

We can write the position of the sphere's contact point (with the ground) as the sum of the distance from the inertial frame, $\vec{\mathcal{F}}_{\mathrm{i}}$, to the sphere frame, $\vec{\mathcal{F}}_{\mathrm{s}}$, to the contact point as

$$\vec{\mathbf{r}}^{\mathrm{ci}} = \vec{\mathbf{r}}^{\mathrm{si}} + \vec{\mathbf{r}}^{\mathrm{cs}}$$

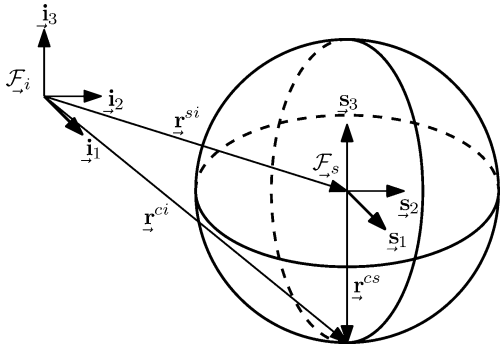

Fig. 3 Sphere rolling (pendulum not drawn)

[2] Quasi-coordinates are those which are not integrable, and a general angular velocity such as $\boldsymbol{\omega}_{\mathrm{s}}^{\mathrm{si}}$ is not integrable, that is, $\int_0^t \boldsymbol{\omega}_{\mathrm{s}}^{\mathrm{si}}(\tau)\, d\tau \neq \boldsymbol{\theta}^{\mathrm{si}}(t) - \boldsymbol{\theta}^{\mathrm{si}}(0)$.

where $\underset{\rightarrow}{\mathbf{r}}^{\mathrm{si}} = \underset{\rightarrow}{\mathcal{F}}_{\mathrm{i}}^{\mathrm{T}} \mathbf{r}_{\mathrm{i}}^{\mathrm{si}}$, $\mathbf{r}_{\mathrm{i}}^{\mathrm{si}} = [x \ y \ z]^{\mathrm{T}}$, $\underset{\rightarrow}{\mathbf{r}}^{\mathrm{cs}} = \underset{\rightarrow}{\mathcal{F}}_{\mathrm{i}}^{\mathrm{T}} \mathbf{r}_{\mathrm{i}}^{\mathrm{cs}}$, $\mathbf{r}_{\mathrm{i}}^{\mathrm{cs}} = [0 \ 0 \ -r]^{\mathrm{T}}$ and r is the radius of the sphere. The time derivative of the position of the contact point is

$$\begin{aligned}
\underset{\rightarrow}{\dot{\mathbf{r}}}^{\mathrm{ci}} &= \underset{\rightarrow}{\dot{\mathbf{r}}}^{\mathrm{si}} + \underset{\rightarrow}{\dot{\mathbf{r}}}^{\mathrm{cs}} \\
&= \underset{\rightarrow}{\dot{\mathbf{r}}}^{\mathrm{si}} + \underset{\rightarrow}{\boldsymbol{\omega}}_{\mathrm{s}}^{\mathrm{si}} \times \underset{\rightarrow}{\mathbf{r}}^{\mathrm{cs}} \\
&= \underset{\rightarrow}{\mathcal{F}}_{\mathrm{i}}^{\mathrm{T}} \left(\dot{\mathbf{r}}_{\mathrm{i}}^{\mathrm{si}} + \left(\mathbf{C}_{\mathrm{si}}^{\mathrm{T}} \boldsymbol{\omega}_{\mathrm{s}}^{\mathrm{si}} \right)^{\times} \mathbf{r}_{\mathrm{i}}^{\mathrm{cs}} \right) \\
&= \underset{\rightarrow}{\mathcal{F}}_{\mathrm{i}}^{\mathrm{T}} \left(\dot{\mathbf{r}}_{\mathrm{i}}^{\mathrm{si}} + r \mathbf{z}^{\times} \mathbf{C}_{\mathrm{si}}^{\mathrm{T}} \boldsymbol{\omega}_{\mathrm{s}}^{\mathrm{si}} \right)
\end{aligned}$$

where $\mathbf{C}_{\mathrm{si}}$ is the rotation matrix from $\underset{\rightarrow}{\mathcal{F}}_{\mathrm{i}}$ to $\underset{\rightarrow}{\mathcal{F}}_{\mathrm{s}}$. The instantaneous velocity of the contact point is zero, i.e., $\dot{\mathbf{r}}_{\mathrm{i}}^{\mathrm{ci}} \equiv \mathbf{0}$. Therefore, we have

$$\dot{\mathbf{r}}_{\mathrm{i}}^{\mathrm{si}} = -r \mathbf{z}^{\times} \mathbf{C}_{\mathrm{si}}^{\mathrm{T}} \mathbf{S}_{\mathrm{s}}^{\mathrm{si}} \dot{\boldsymbol{\theta}}^{\mathrm{si}} = -r \mathbf{z}^{\times} \mathbf{C}_{\mathrm{si}}^{\mathrm{T}} \boldsymbol{\omega}_{\mathrm{s}}^{\mathrm{si}}. \tag{1}$$

Equation (1) is the relation between the sphere's Euler angle rates $\dot{\boldsymbol{\theta}}^{\mathrm{si}}$ and translational velocity $\dot{\mathbf{r}}_{\mathrm{i}}^{\mathrm{si}}$. It is also the relation between $\boldsymbol{\omega}_{\mathrm{s}}^{\mathrm{si}}$ and $\dot{\mathbf{r}}_{\mathrm{i}}^{\mathrm{si}}$. It is a non-holonomic constraint that must always be satisfied.

5.2.2 Pendulum constraint

Consider the angular velocity of the payload frame with respect to the sphere frame:

$$\boldsymbol{\omega}_{\mathrm{p}}^{\mathrm{pi}} = \boldsymbol{\omega}_{\mathrm{p}}^{\mathrm{ps}} + \mathbf{C}_{\mathrm{ps}} \boldsymbol{\omega}_{\mathrm{s}}^{\mathrm{si}} \quad \Leftrightarrow \quad \boldsymbol{\omega}_{\mathrm{p}}^{\mathrm{ps}} = \boldsymbol{\omega}_{\mathrm{p}}^{\mathrm{pi}} - \mathbf{C}_{\mathrm{ps}} \boldsymbol{\omega}_{\mathrm{s}}^{\mathrm{si}} \tag{2}$$

where $\mathbf{C}_{\mathrm{ps}} = \mathbf{C}_{\mathrm{pi}} \mathbf{C}_{\mathrm{si}}^{\mathrm{T}}$. As previously mentioned, the pendulum will be constrained such that the $\underset{\rightarrow}{\mathbf{s}}_2$-axis of the sphere frame and the $\underset{\rightarrow}{\mathbf{p}}_2$-axis of the payload frame are coincident. This constraint implies that the angular velocity of the payload with respect to the sphere is zero in the $\underset{\rightarrow}{\mathbf{p}}_1$ and $\underset{\rightarrow}{\mathbf{p}}_3$ directions and non-zero about $\underset{\rightarrow}{\mathbf{p}}_2$. Therefore, $\omega_{\mathrm{p},1}^{\mathrm{ps}} = \omega_{\mathrm{p},3}^{\mathrm{ps}} = 0$, and $\omega_{\mathrm{p},2}^{\mathrm{ps}} \neq 0$. Employing (2), the constraint on the pendulum's angular velocity can be expressed mathematically as

$$\begin{aligned}
&[\mathbf{x} \quad \mathbf{0} \quad \mathbf{z}] \boldsymbol{\omega}_{\mathrm{p}}^{\mathrm{ps}} = \mathbf{0} \\
&\Leftrightarrow \quad \left(-[\mathbf{x} \quad \mathbf{0} \quad \mathbf{z}] \mathbf{C}_{\mathrm{ps}} \quad [\mathbf{x} \quad \mathbf{0} \quad \mathbf{z}] \right) \begin{bmatrix} \boldsymbol{\omega}_{\mathrm{s}}^{\mathrm{si}} \\ \boldsymbol{\omega}_{\mathrm{p}}^{\mathrm{pi}} \end{bmatrix} = \mathbf{0}.
\end{aligned} \tag{3}$$

The pendulum constraint is also non-holonomic.

5.2.3 Combining the non-holonomic constraints

We can combine the rolling constraint and the pendulum constraint as follows:

$$\underbrace{\begin{bmatrix} \mathbf{1} & r \mathbf{z}^{\times} \mathbf{C}_{\mathrm{si}}^{\mathrm{T}} \mathbf{S}_{\mathrm{s}}^{\mathrm{si}} & \mathbf{0} \\ \mathbf{0} & -[\mathbf{x} \quad \mathbf{0} \quad \mathbf{z}] \mathbf{C}_{\mathrm{ps}} \mathbf{S}_{\mathrm{s}}^{\mathrm{si}} & [\mathbf{x} \quad \mathbf{0} \quad \mathbf{z}] \mathbf{S}_{\mathrm{p}}^{\mathrm{pi}} \end{bmatrix}}_{\boldsymbol{\Xi}} \underbrace{\begin{bmatrix} \dot{\mathbf{r}}_{\mathrm{i}}^{\mathrm{si}} \\ \dot{\boldsymbol{\theta}}^{\mathrm{si}} \\ \dot{\boldsymbol{\theta}}^{\mathrm{pi}} \end{bmatrix}}_{\dot{\mathbf{q}}} = \mathbf{0} \quad \Leftrightarrow \quad \boldsymbol{\Xi} \dot{\mathbf{q}} = \mathbf{0}. \tag{4}$$

The column matrix $\mathbf{q}$ will be referred to as the dependent generalized coordinates. Note that $\dot{\mathbf{q}}$ lies in the Null space (or Kernel) of $\boldsymbol{\Xi}$. The matrix $\boldsymbol{\Xi}$ has a dimension of 6×9, and is of rank 5.

5.2.4 Properties of the non-holonomic constraints

The pendulum constraint forces the pendulum and the sphere's central-rod to remain perpendicular to each other at all times. It follows that the corresponding rotation matrix from the sphere frame to the payload frame is simply a single rotation about the $\underset{\rightarrow}{\mathbf{s}}_2$-axis, $\mathbf{C}_{\mathrm{ps}} \equiv \mathbf{C}_2(\phi)$, where the angle ϕ is the rotation angle [19].

Knowing that there is only one rotation that distinguishes $\underset{\rightarrow}{\mathcal{F}}_{\mathrm{p}}$ from $\underset{\rightarrow}{\mathcal{F}}_{\mathrm{s}}$ we can express $\boldsymbol{\omega}_{\mathrm{p}}^{\mathrm{pi}}$ in terms of $\boldsymbol{\omega}_{\mathrm{s}}^{\mathrm{si}}$ and $\dot{\phi}$:

$$\boldsymbol{\omega}_{\mathrm{p}}^{\mathrm{pi}} = \mathbf{y}\dot{\phi} + \mathbf{C}_{\mathrm{ps}}\boldsymbol{\omega}_{\mathrm{s}}^{\mathrm{si}} \quad \Leftrightarrow \quad \dot{\boldsymbol{\theta}}^{\mathrm{pi}} = \mathbf{S}_{\mathrm{p}}^{\mathrm{pi}\,-1}\mathbf{y}\dot{\phi} + \mathbf{S}_{\mathrm{p}}^{\mathrm{pi}\,-1}\mathbf{C}_{\mathrm{ps}}\mathbf{S}_{\mathrm{s}}^{\mathrm{si}}\dot{\boldsymbol{\theta}}^{\mathrm{si}} \tag{5}$$

where $\mathbf{y}\dot{\phi} = \boldsymbol{\omega}_{\mathrm{p}}^{\mathrm{ps}}$. Although we can express the system in terms of the dependent generalized coordinates, we can also express the system in terms of a set of reduced, or independent generalized coordinates by observing that $\dot{\mathbf{r}}_{\mathrm{i}}^{\mathrm{si}}$ depends on $\dot{\boldsymbol{\theta}}^{\mathrm{si}}$, and $\dot{\boldsymbol{\theta}}^{\mathrm{pi}}$ depends on $\dot{\boldsymbol{\theta}}^{\mathrm{si}}$ and $\dot{\phi}$. By augmenting (1) and (5), we have

$$\begin{bmatrix} \dot{\mathbf{r}}_{\mathrm{i}}^{\mathrm{si}} \\ \dot{\boldsymbol{\theta}}^{\mathrm{si}} \\ \dot{\boldsymbol{\theta}}^{\mathrm{pi}} \end{bmatrix} = \underbrace{\begin{bmatrix} -r\mathbf{z}^{\times}\mathbf{C}_{\mathrm{si}}^{\mathrm{T}}\mathbf{S}_{\mathrm{s}}^{\mathrm{si}} & \mathbf{0} \\ \mathbf{1} & \mathbf{0} \\ \mathbf{S}_{\mathrm{p}}^{\mathrm{pi}\,-1}\mathbf{C}_{\mathrm{ps}}\mathbf{S}_{\mathrm{s}}^{\mathrm{si}} & \mathbf{S}_{\mathrm{p}}^{\mathrm{pi}\,-1}\mathbf{y} \end{bmatrix}}_{\boldsymbol{\Upsilon}} \underbrace{\begin{bmatrix} \dot{\boldsymbol{\theta}}^{\mathrm{si}} \\ \dot{\phi} \end{bmatrix}}_{\dot{\hat{\mathbf{q}}}} \quad \Leftrightarrow \quad \dot{\mathbf{q}} = \boldsymbol{\Upsilon}\dot{\hat{\mathbf{q}}} \tag{6}$$

where $\hat{\mathbf{q}}$ will be referred to as the independent generalized coordinates and $\boldsymbol{\Upsilon}$ is the mapping between the independent generalized coordinates and the dependent generalized coordinates.

A key feature of $\boldsymbol{\Upsilon}$ and $\boldsymbol{\Xi}$ which will be exploited in the future is the following relation:

$$\boldsymbol{\Xi}\dot{\mathbf{q}} = \boldsymbol{\Xi}\boldsymbol{\Upsilon}\dot{\hat{\mathbf{q}}} = \mathbf{0} \quad \Rightarrow \quad \boldsymbol{\Xi}\boldsymbol{\Upsilon} = \mathbf{0} \quad \Leftrightarrow \quad \boldsymbol{\Upsilon}^{\mathrm{T}}\boldsymbol{\Xi}^{\mathrm{T}} = \mathbf{0}. \tag{7}$$

The above result can be shown by straightforward algebra, and is left to the reader. The matrix $\boldsymbol{\Upsilon}$ has a dimension of 9×4, and is of rank 4. Note that $\mathrm{rank}(\boldsymbol{\Xi}) + \mathrm{rank}(\boldsymbol{\Upsilon}) = 9$, which is equal to the number of dependent generalized coordinates.

5.3 Other useful kinematic relations

In the interest of keeping our dynamic derivation concise, we will define various augmented kinematic relations. To start, the augmented dependent velocities can be written as

$$\dot{\mathbf{r}} := \begin{bmatrix} \dot{\mathbf{r}}_{\mathrm{i}}^{\mathrm{si}} \\ \boldsymbol{\omega}_{\mathrm{s}}^{\mathrm{si}} \\ \boldsymbol{\omega}_{\mathrm{p}}^{\mathrm{pi}} \end{bmatrix} = \underbrace{\begin{bmatrix} \mathbf{1} & \mathbf{0} & \mathbf{0} \\ \mathbf{0} & \mathbf{S}_{\mathrm{s}}^{\mathrm{si}} & \mathbf{0} \\ \mathbf{0} & \mathbf{0} & \mathbf{S}_{\mathrm{p}}^{\mathrm{pi}} \end{bmatrix}}_{\bar{\mathbf{S}}} \begin{bmatrix} \dot{\mathbf{r}}_{\mathrm{i}}^{\mathrm{si}} \\ \dot{\boldsymbol{\theta}}^{\mathrm{si}} \\ \dot{\boldsymbol{\theta}}^{\mathrm{pi}} \end{bmatrix} \quad \Leftrightarrow \quad \dot{\mathbf{r}} = \bar{\mathbf{S}}\dot{\mathbf{q}}$$

where $\bar{\mathbf{S}}$ is the augmented mapping matrix. We will also define

$$\dot{\mathbf{r}}^{\times} := \begin{bmatrix} \dot{\mathbf{r}}_{\mathrm{i}}^{\mathrm{si}\times} & \mathbf{0} & \mathbf{0} \\ \mathbf{0} & \boldsymbol{\omega}_{\mathrm{s}}^{\mathrm{si}\times} & \mathbf{0} \\ \mathbf{0} & \mathbf{0} & \boldsymbol{\omega}_{\mathrm{p}}^{\mathrm{pi}\times} \end{bmatrix}$$

which is the augmented cross matrix of the augmented dependent velocities. Expressing (1) and (5) in terms of angular velocities (rather than in terms of Euler angle rates as we did in (6)), we can write

$$\begin{bmatrix} \dot{\mathbf{r}}_{\mathrm{i}}^{\mathrm{si}} \\ \boldsymbol{\omega}_{\mathrm{s}}^{\mathrm{si}} \\ \boldsymbol{\omega}_{\mathrm{p}}^{\mathrm{pi}} \end{bmatrix} = \underbrace{\begin{bmatrix} -r\mathbf{z}^{\times}\mathbf{C}_{\mathrm{si}}^{\mathrm{T}} & \mathbf{0} \\ \mathbf{1} & \mathbf{0} \\ \mathbf{C}_{\mathrm{ps}} & \mathbf{y} \end{bmatrix}}_{\boldsymbol{\Pi}} \underbrace{\begin{bmatrix} \boldsymbol{\omega}_{\mathrm{s}}^{\mathrm{si}} \\ \dot{\phi} \end{bmatrix}}_{\hat{\boldsymbol{\omega}}} \quad \Leftrightarrow \quad \dot{\mathbf{r}} = \boldsymbol{\Pi}\hat{\boldsymbol{\omega}} \tag{8}$$

where $\hat{\boldsymbol{\omega}}$ are the augmented independent velocities and $\boldsymbol{\Pi}$ is the map between the augmented independent velocities and the augmented dependent velocities. The relation between $\hat{\boldsymbol{\omega}}$ and $\dot{\hat{\mathbf{q}}}$ is

$$\begin{bmatrix} \boldsymbol{\omega}_{\mathrm{s}}^{\mathrm{si}} \\ \dot{\phi} \end{bmatrix} = \underbrace{\begin{bmatrix} \mathbf{S}_{\mathrm{s}}^{\mathrm{si}} & \mathbf{0} \\ \mathbf{0} & 1 \end{bmatrix}}_{\hat{\mathbf{S}}} \begin{bmatrix} \dot{\boldsymbol{\theta}}^{\mathrm{si}} \\ \dot{\phi} \end{bmatrix}.$$

It can be shown that $\boldsymbol{\Upsilon} = \bar{\mathbf{S}}^{-1}\boldsymbol{\Pi}\hat{\mathbf{S}}$. The temporal derivative of (8) will also be needed in the future:

$$\ddot{\mathbf{r}} = \dot{\boldsymbol{\Pi}}\hat{\boldsymbol{\omega}} + \boldsymbol{\Pi}\dot{\hat{\boldsymbol{\omega}}} \tag{9}$$

where

$$\dot{\boldsymbol{\Pi}} = \begin{bmatrix} -r\mathbf{z}^{\times}\dot{\mathbf{C}}_{\mathrm{si}}^{\mathrm{T}} & \mathbf{0} \\ \mathbf{0} & \mathbf{0} \\ \dot{\mathbf{C}}_{\mathrm{ps}} & \mathbf{0} \end{bmatrix} = \begin{bmatrix} -r\mathbf{z}^{\times}\mathbf{C}_{\mathrm{si}}^{\mathrm{T}}\boldsymbol{\omega}_{\mathrm{s}}^{\mathrm{si}\times} & \mathbf{0} \\ \mathbf{0} & \mathbf{0} \\ -\dot{\phi}\mathbf{y}^{\times}\mathbf{C}_{\mathrm{ps}} & \mathbf{0} \end{bmatrix}.$$

In the above simplification, we have used Poisson's equation which relates the temporal derivative of a rotation matrix to angular velocity:

$$\dot{\mathbf{C}}_{\mathrm{si}} + \boldsymbol{\omega}_{\mathrm{s}}^{\mathrm{si}\times}\mathbf{C}_{\mathrm{si}} = \mathbf{0}, \qquad \dot{\mathbf{C}}_{\mathrm{pi}} + \boldsymbol{\omega}_{\mathrm{p}}^{\mathrm{pi}\times}\mathbf{C}_{\mathrm{pi}} = \mathbf{0}, \qquad \dot{\mathbf{C}}_{\mathrm{ps}} + \dot{\phi}\mathbf{y}^{\times}\mathbf{C}_{\mathrm{ps}} = \mathbf{0}.$$

6 The method of virtual work and the generalized forces and torques

We will consider three external forces: $\mathbf{t}^{\mathrm{f}}$, $\mathbf{t}^{\mathrm{w}}$, and $\mathbf{t}^{\mathrm{p}}$ which represent the generalized rolling resistance, induced wind force, and power generation torque. In order to calculate these forces, we will use the method of virtual work, which will concern us with virtual displacements associated with $\mathbf{r}_{\mathrm{i}}^{\mathrm{si}}$ and virtual angular displacements associated with $\boldsymbol{\theta}^{\mathrm{si}}$ and $\boldsymbol{\theta}^{\mathrm{pi}}$.

6.1 Rolling friction

We will first consider rolling friction, which can be modeled as viscous damping. We will separate the rolling friction into translational damping and spin damping.

The translational damping will be modeled as follows

$$\underset{\rightarrow}{\mathbf{f}}^{\mathrm{r}} = \underset{\rightarrow}{\mathcal{F}}_{\mathrm{i}}^{\mathrm{T}}\left(-b_{\mathrm{r}}\dot{\mathbf{r}}_{\mathrm{i}}^{\mathrm{si}}\right) = \underset{\rightarrow}{\mathcal{F}}_{\mathrm{i}}^{\mathrm{T}}\mathbf{f}_{\mathrm{i}}^{\mathrm{r}}$$

where b_{r} is the translational, or rolling damping factor and $\dot{\mathbf{r}}_{\mathrm{i}}^{\mathrm{si}} = -r\mathbf{z}^{\times}\mathbf{C}_{\mathrm{si}}^{\mathrm{T}}\boldsymbol{\omega}_{\mathrm{s}}^{\mathrm{si}}$, as presented in (1). The virtual work done due to translational damping is then

$$\delta W = \underset{\rightarrow}{\mathbf{f}}^{\mathrm{r}} \cdot \delta\underset{\rightarrow}{\mathbf{r}}^{\mathrm{si}} = \mathbf{f}_{\mathrm{i}}^{\mathrm{r}\mathrm{T}}\delta\mathbf{r}_{\mathrm{i}}^{\mathrm{si}} = \underbrace{\begin{bmatrix}\delta\mathbf{r}^{\mathrm{si}\mathrm{T}} & \delta\boldsymbol{\theta}^{\mathrm{si}\mathrm{T}} & \delta\boldsymbol{\theta}^{\mathrm{pi}\mathrm{T}}\end{bmatrix}}_{\delta\mathbf{q}^{\mathrm{T}}}\begin{bmatrix}\mathbf{1} & \mathbf{0} & \mathbf{0}\\ \mathbf{0} & \mathbf{S}_{\mathrm{s}}^{\mathrm{si}\mathrm{T}} & \mathbf{0}\\ \mathbf{0} & \mathbf{0} & \mathbf{S}_{\mathrm{p}}^{\mathrm{pi}\mathrm{T}}\end{bmatrix}\underbrace{\begin{bmatrix}\mathbf{f}_{\mathrm{i}}^{\mathrm{r}}\\ \mathbf{0}\\ \mathbf{0}\end{bmatrix}}_{\mathbf{f}^{\mathrm{r}}} = \delta\mathbf{q}^{\mathrm{T}}\bar{\mathbf{S}}^{\mathrm{T}}\mathbf{f}^{\mathrm{r}} = \delta\mathbf{q}^{\mathrm{T}}\mathbf{t}^{\mathrm{r}}$$

where $\mathbf{t}^{\mathrm{r}} = \bar{\mathbf{S}}^{\mathrm{T}}\mathbf{f}^{\mathrm{r}}$ is the generalized force due to translational damping.

The above expression for translational damping mostly has a dissipating effect on the first two elements of $\boldsymbol{\omega}_{\mathrm{s}}^{\mathrm{si}}$ (i.e., $\omega_{\mathrm{s},1}^{\mathrm{si}}$ and $\omega_{\mathrm{s},2}^{\mathrm{si}}$) through the constraint $\dot{\mathbf{r}}_{\mathrm{i}}^{\mathrm{si}} = -r\mathbf{z}^{\times}\mathbf{C}_{\mathrm{si}}^{\mathrm{T}}\boldsymbol{\omega}_{\mathrm{s}}^{\mathrm{si}}$. To ensure that the ball is sufficiently damped, we must include some sort of 'contact patch' friction, to ensure that the system will be damped if the ball-pendulum system were to have significant angular velocity in the $\underset{\rightarrow}{\mathbf{i}}_3$ direction of the $\underset{\rightarrow}{\mathcal{F}}_{\mathrm{i}}$ frame.[3] Consider the following torque created via 'spin damping'

$$\underset{\rightarrow}{\boldsymbol{\tau}}^{\mathrm{s}} = \underset{\rightarrow}{\mathcal{F}}_{\mathrm{s}}^{\mathrm{T}}\mathbf{C}_{\mathrm{si}}\mathbf{z}\left(-b_{\mathrm{s}}\mathbf{z}^{\mathrm{T}}\right)\mathbf{C}_{\mathrm{si}}^{\mathrm{T}}\boldsymbol{\omega}_{s}^{\mathrm{si}} = \underset{\rightarrow}{\mathcal{F}}_{\mathrm{s}}^{\mathrm{T}}\left(-b_{\mathrm{s}}\mathbf{C}_{\mathrm{si}}\mathbf{z}\mathbf{z}^{\mathrm{T}}\mathbf{C}_{\mathrm{si}}^{\mathrm{T}}\boldsymbol{\omega}_{\mathrm{s}}^{\mathrm{si}}\right) = \underset{\rightarrow}{\mathcal{F}}_{\mathrm{s}}^{\mathrm{T}}\boldsymbol{\tau}_{\mathrm{s}}^{\mathrm{s}}$$

where b_{s} is the spin damping coefficient. The virtual work done due to spin damping is then

$$\delta W = \underset{\rightarrow}{\boldsymbol{\tau}}^{\mathrm{s}} \cdot \left(\underset{\rightarrow}{\mathcal{F}}_{\mathrm{s}}^{\mathrm{T}}\mathbf{S}_{\mathrm{s}}^{\mathrm{si}}\delta\boldsymbol{\theta}^{\mathrm{si}}\right) = \delta\boldsymbol{\theta}^{\mathrm{si}\mathrm{T}}\mathbf{S}_{\mathrm{s}}^{\mathrm{si}\mathrm{T}}\boldsymbol{\tau}_{\mathrm{s}}^{\mathrm{s}} = \delta\mathbf{q}^{\mathrm{T}}\bar{\mathbf{S}}^{\mathrm{T}}\underbrace{\begin{bmatrix}\mathbf{0}\\ \boldsymbol{\tau}_{\mathrm{s}}^{\mathrm{s}}\\ \mathbf{0}\end{bmatrix}}_{\boldsymbol{\tau}^{\mathrm{s}}} = \delta\mathbf{q}^{\mathrm{T}}\bar{\mathbf{S}}^{\mathrm{T}}\boldsymbol{\tau}^{\mathrm{s}} = \delta\mathbf{q}^{\mathrm{T}}\mathbf{t}^{\mathrm{s}}$$

where $\mathbf{t}^{\mathrm{s}} = \bar{\mathbf{S}}^{\mathrm{T}}\boldsymbol{\tau}^{\mathrm{s}}$ is the generalized force due to spin damping.

Therefore, the total damping induced is

$$\mathbf{t}^{\mathrm{f}} = \mathbf{t}^{\mathrm{r}} + \mathbf{t}^{\mathrm{s}} = \bar{\mathbf{S}}^{\mathrm{T}}\boldsymbol{\tau}^{\mathrm{f}}$$

where $\boldsymbol{\tau}^{\mathrm{f}} = \mathbf{f}^{\mathrm{r}} + \boldsymbol{\tau}^{\mathrm{s}}$ is the generalized damping force due to friction.

6.2 Wind force

To simplify our analysis we assume that the force applied to the ball as a result of wind can be modeled by the simple aerodynamic drag associated with a sphere in a fluid [20]

$$\underset{\rightarrow}{\mathbf{f}}^{\mathrm{w}} = \underset{\rightarrow}{\mathcal{F}}_{\mathrm{i}}^{\mathrm{T}}\left(\frac{1}{2}\rho A C_{\mathrm{d}} v^2 \hat{\mathbf{v}}_{\mathrm{i}}\right) = \underset{\rightarrow}{\mathcal{F}}_{\mathrm{i}}^{\mathrm{T}}\mathbf{f}_{\mathrm{i}}^{\mathrm{w}}$$

[3] Note that $\mathbf{z}^{\times}\mathbf{z} = \mathbf{0}$ and Rank $\mathbf{z}^{\times} = 2$, that is $\mathbf{z}^{\times}$ has a Null space of dimension one. Any angular velocity parallel to $\mathbf{z}$, that is any $\boldsymbol{\omega}_{\mathrm{i}}^{\mathrm{si}} = \mathbf{C}_{\mathrm{si}}^{\mathrm{T}}\boldsymbol{\omega}_{\mathrm{s}}^{\mathrm{si}} \in \mathrm{Ker}(\mathbf{z}^{\times})$, will not be dampened by $\mathbf{f}^{\mathrm{r}}$.

where ρ is the density of the surrounding fluid, A is the frontal area of the ball, C_d is the drag coefficient, v is the velocity of the fluid relative to the ball's motion, and $\hat{\mathbf{v}}_\mathrm{i}$ is a unit vector representing the direction of the wind's velocity. In this paper, we will neglect any sort of 'ground effect' the fluid may have due to interaction with the ground, and assume that the force associated with the wind is applied directly at the center of the ball.

The virtual work done due to the induced wind force is then

$$\delta W = \underset{\rightarrow}{\mathbf{f}}^\mathrm{w} \cdot \delta \underset{\rightarrow}{\mathbf{r}}^\mathrm{si} = \delta \mathbf{r}_\mathrm{i}^{\mathrm{si}\,\mathrm{T}} \mathbf{f}_\mathrm{i}^\mathrm{w} = \delta \mathbf{q}^\mathrm{T} \bar{\mathbf{S}}^\mathrm{T} \underbrace{\begin{bmatrix} \mathbf{f}_\mathrm{i}^\mathrm{w} \\ \mathbf{0} \\ \mathbf{0} \end{bmatrix}}_{\mathbf{f}^\mathrm{w}} = \delta \mathbf{q}^\mathrm{T} \bar{\mathbf{S}}^\mathrm{T} \mathbf{f}^\mathrm{w} = \delta \mathbf{q}^\mathrm{T} \mathbf{t}^\mathrm{w}$$

where $\mathbf{t}^\mathrm{w} = \bar{\mathbf{S}}^\mathrm{T} \mathbf{f}^\mathrm{w}$ is the generalized induced wind force.

6.3 Power generation

As the sphere rolls, a torque about the $\underset{\rightarrow}{\mathbf{p}}_2$-axis is created as a result of on-board power generation. The amount of power generated will be proportional to the relative angular velocity between the payload and sphere about the $\underset{\rightarrow}{\mathbf{p}}_2$-axis and said torque. The torque created about the $\underset{\rightarrow}{\mathbf{p}}_2$-axis is

$$\underset{\rightarrow}{\boldsymbol{\tau}}^\mathrm{p} = \underset{\rightarrow}{\mathcal{F}}_\mathrm{p}^\mathrm{T} \begin{bmatrix} 0 \\ -b_\mathrm{p} \dot{\phi} \\ 0 \end{bmatrix} = \underset{\rightarrow}{\mathcal{F}}_\mathrm{p}^\mathrm{T} \boldsymbol{\tau}_\mathrm{p}^\mathrm{p}.$$

If we note that $\boldsymbol{\omega}_\mathrm{p}^\mathrm{ps} = \mathbf{S}_\mathrm{p}^\mathrm{pi} \dot{\boldsymbol{\theta}}^\mathrm{pi} - \mathbf{C}_\mathrm{ps} \mathbf{S}_\mathrm{s}^\mathrm{si} \dot{\boldsymbol{\theta}}^\mathrm{si}$, then it follows that the virtual work done due to on-board power generation is

$$\begin{aligned}
\delta W &= \underset{\rightarrow}{\boldsymbol{\tau}}^\mathrm{p} \cdot \left(\underset{\rightarrow}{\mathcal{F}}_\mathrm{p}^\mathrm{T} \mathbf{S}_\mathrm{p}^\mathrm{pi} \delta \boldsymbol{\theta}^\mathrm{pi} - \underset{\rightarrow}{\mathcal{F}}_\mathrm{p}^\mathrm{T} \mathbf{C}_\mathrm{ps} \mathbf{S}_\mathrm{s}^\mathrm{si} \delta \boldsymbol{\theta}^\mathrm{si} \right) \\
&= \delta \boldsymbol{\theta}^{\mathrm{pi}\,\mathrm{T}} \mathbf{S}_\mathrm{p}^{\mathrm{pi}\,\mathrm{T}} \boldsymbol{\tau}_\mathrm{p}^\mathrm{p} - \delta \boldsymbol{\theta}^{\mathrm{si}\,\mathrm{T}} \mathbf{S}_\mathrm{s}^{\mathrm{si}\,\mathrm{T}} \mathbf{C}_\mathrm{ps}^\mathrm{T} \boldsymbol{\tau}_\mathrm{p}^\mathrm{p} \\
&= \delta \mathbf{q}^\mathrm{T} \bar{\mathbf{S}}^\mathrm{T} \begin{bmatrix} \mathbf{0} \\ -\mathbf{C}_\mathrm{ps}^\mathrm{T} \boldsymbol{\tau}_\mathrm{p}^\mathrm{p} \\ \boldsymbol{\tau}_\mathrm{p}^\mathrm{p} \end{bmatrix} \\
&= \delta \mathbf{q}^\mathrm{T} \bar{\mathbf{S}}^\mathrm{T} \boldsymbol{\tau}^\mathrm{p} \\
&= \delta \mathbf{q}^\mathrm{T} \mathbf{t}^\mathrm{p}
\end{aligned}$$

where $\mathbf{t}^\mathrm{p} = \bar{\mathbf{S}}^\mathrm{T} \boldsymbol{\tau}^\mathrm{p}$ is the generalized force due to on-board power generation.

7 Deriving the equations of motion

7.1 Kinetic energy

7.1.1 Kinetic energy of sphere

We will assume that the sphere has a uniform thickness, and we will ignore the mass and inertia associated with of the sphere's central rod. Consider a small mass element of the

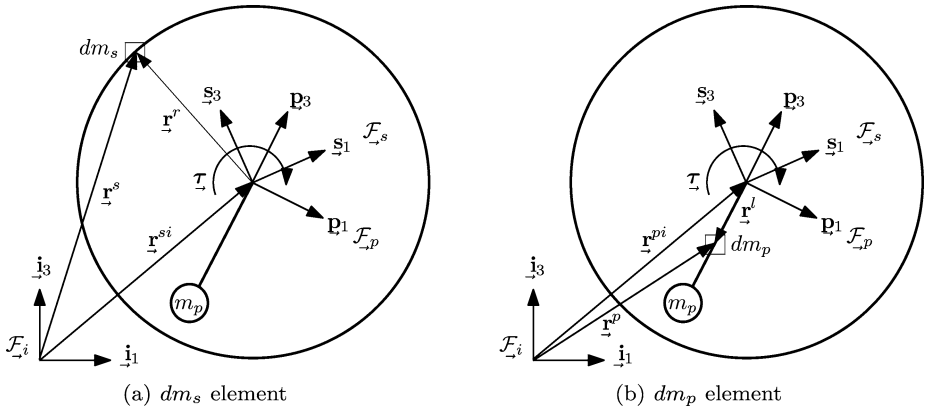

Fig. 4 Tumbleweed rover side view, mass elements dm_s and dm_p

sphere, dm_s, shown in Fig. 4(a). The position of dm_s is

$$\vec{\mathbf{r}}^{\,\mathrm{s}} = \vec{\mathbf{r}}^{\,\mathrm{si}} + \vec{\mathbf{r}}^{\,\mathrm{r}} = \vec{\mathcal{F}}_s^{\mathrm{T}}\left(\mathbf{C}_{\mathrm{si}}\mathbf{r}_{\mathrm{i}}^{\mathrm{si}} + \mathbf{r}_{\mathrm{s}}^{\mathrm{r}}\right).$$

The velocity of the mass element is then

$$\dot{\vec{\mathbf{r}}}^{\,\mathrm{s}} = \dot{\vec{\mathbf{r}}}^{\,\mathrm{si}} + \dot{\vec{\mathbf{r}}}^{\,\mathrm{r}} = \vec{\mathcal{F}}_s^{\mathrm{T}}\left(\mathbf{C}_{\mathrm{si}}\dot{\mathbf{r}}_{\mathrm{i}}^{\mathrm{si}} - \mathbf{r}_{\mathrm{s}}^{\mathrm{r}\times}\boldsymbol{\omega}_{\mathrm{s}}^{\mathrm{si}}\right).$$

The kinetic energy of the ball can then be written as

$$T_\mathrm{s} = \frac{1}{2}\int_{\mathcal{B}} \dot{\vec{\mathbf{r}}}^{\,\mathrm{s}} \cdot \dot{\vec{\mathbf{r}}}^{\,\mathrm{s}}\, dm_\mathrm{s} = \frac{1}{2}\begin{bmatrix}\dot{\mathbf{r}}_{\mathrm{i}}^{\mathrm{si}\mathrm{T}} & \boldsymbol{\omega}_{\mathrm{s}}^{\mathrm{si}\mathrm{T}}\end{bmatrix}\begin{bmatrix} m_\mathrm{s}\mathbf{1} & \mathbf{0} \\ \mathbf{0} & \mathbf{J}_\mathrm{s}\end{bmatrix}\begin{bmatrix}\dot{\mathbf{r}}_{\mathrm{i}}^{\mathrm{si}} \\ \boldsymbol{\omega}_{\mathrm{s}}^{\mathrm{si}}\end{bmatrix}$$

where $\mathbf{J}_\mathrm{s} = -\int_{\mathcal{B}} \mathbf{r}_{\mathrm{s}}^{\mathrm{r}\times}\mathbf{r}_{\mathrm{s}}^{\mathrm{r}\times}\, dm_\mathrm{s}$ and the integral is evaluated over the body, $\mathcal{B}$. Note that $\int_{\mathcal{B}} \mathbf{r}_{\mathrm{s}}^{\mathrm{r}}\, dm_\mathrm{s} = \mathbf{0}$, that is to say there is no first moment of mass, $\mathbf{c}_\mathrm{s}$, associated with the sphere.

7.1.2 Kinetic energy of pendulum/payload

Next, consider a small mass element of the payload, dm_p, shown in Fig. 4(b). The position of the point mass dm_p is

$$\vec{\mathbf{r}}^{\,\mathrm{p}} = \vec{\mathbf{r}}^{\,\mathrm{pi}} + \vec{\mathbf{r}}^{\,\mathrm{l}} = \vec{\mathcal{F}}_p^{\mathrm{T}}\left(\mathbf{C}_{\mathrm{pi}}\mathbf{r}_{\mathrm{i}}^{\mathrm{pi}} + \mathbf{r}_{\mathrm{p}}^{\mathrm{l}}\right).$$

The velocity of the mass element is then

$$\dot{\vec{\mathbf{r}}}^{\,\mathrm{p}} = \dot{\vec{\mathbf{r}}}^{\,\mathrm{pi}} + \dot{\vec{\mathbf{r}}}^{\,\mathrm{l}} = \vec{\mathcal{F}}_p^{\mathrm{T}}\left(\mathbf{C}_{\mathrm{pi}}\dot{\mathbf{r}}_{\mathrm{i}}^{\mathrm{pi}} - \mathbf{r}_{\mathrm{p}}^{\mathrm{l}\times}\boldsymbol{\omega}_{\mathrm{p}}^{\mathrm{pi}}\right).$$

The kinetic energy of the payload is then

$$T_\mathrm{p} = \frac{1}{2}\int_{\mathcal{B}} \dot{\vec{\mathbf{r}}}^{\,\mathrm{p}} \cdot \dot{\vec{\mathbf{r}}}^{\,\mathrm{p}}\, dm_\mathrm{p} = \frac{1}{2}\begin{bmatrix}\dot{\mathbf{r}}_{\mathrm{i}}^{\mathrm{pi}\mathrm{T}} & \boldsymbol{\omega}_{\mathrm{p}}^{\mathrm{pi}\mathrm{T}}\end{bmatrix}\begin{bmatrix} m_\mathrm{p}\mathbf{1} & -\mathbf{C}_{\mathrm{pi}}^{\mathrm{T}}\mathbf{c}_{\mathrm{p}}^{\times} \\ \mathbf{c}_{\mathrm{p}}^{\times}\mathbf{C}_{\mathrm{pi}} & \mathbf{J}_\mathrm{p}\end{bmatrix}\begin{bmatrix}\dot{\mathbf{r}}_{\mathrm{i}}^{\mathrm{pi}} \\ \boldsymbol{\omega}_{\mathrm{p}}^{\mathrm{pi}}\end{bmatrix}$$

where $\mathbf{c}_\mathrm{p} = \int_{\mathcal{B}} \mathbf{r}_{\mathrm{p}}^{\mathrm{l}}\, dm_\mathrm{p}$ and $\mathbf{J}_\mathrm{p} = -\int_{\mathcal{B}} \mathbf{r}_{\mathrm{p}}^{\mathrm{l}\times}\mathbf{r}_{\mathrm{p}}^{\mathrm{l}\times}\, dm_\mathrm{p}$.

7.1.3 Kinetic energy of system

The total kinetic energy of the system is

$$\begin{aligned} T &= T_{\mathrm{s}} + T_{\mathrm{p}} \\ &= \frac{1}{2}\begin{bmatrix} \dot{\mathbf{r}}_{\mathrm{i}}^{\mathrm{pi}\,\mathrm{T}} & \boldsymbol{\omega}_{\mathrm{s}}^{\mathrm{si}\,\mathrm{T}} & \boldsymbol{\omega}_{\mathrm{p}}^{\mathrm{pi}\,\mathrm{T}} \end{bmatrix} \underbrace{\begin{bmatrix} (m_{\mathrm{s}}+m_{\mathrm{p}})\mathbf{1} & \mathbf{0} & -\mathbf{C}_{\mathrm{pi}}^{\mathrm{T}}\mathbf{c}_{\mathrm{p}}^{\times} \\ \mathbf{0} & \mathbf{J}_{\mathrm{s}} & \mathbf{0} \\ \mathbf{c}_{\mathrm{p}}^{\times}\mathbf{C}_{\mathrm{pi}} & \mathbf{0} & \mathbf{J}_{\mathrm{p}} \end{bmatrix}}_{\mathbf{M}(\boldsymbol{\theta}^{\mathrm{pi}})} \begin{bmatrix} \dot{\mathbf{r}}_{\mathrm{i}}^{\mathrm{pi}} \\ \boldsymbol{\omega}_{\mathrm{s}}^{\mathrm{si}} \\ \boldsymbol{\omega}_{\mathrm{p}}^{\mathrm{pi}} \end{bmatrix} \\ &= \frac{1}{2}\dot{\mathbf{r}}^{\mathrm{T}}\mathbf{M}\big(\boldsymbol{\theta}^{\mathrm{pi}}\big)\dot{\mathbf{r}} \\ &= \frac{1}{2}\dot{\mathbf{q}}^{\mathrm{T}}\bar{\mathbf{S}}^{\mathrm{T}}\mathbf{M}\big(\boldsymbol{\theta}^{\mathrm{pi}}\big)\bar{\mathbf{S}}\dot{\mathbf{q}}. \end{aligned} \tag{10}$$

Note that the mass matrix is symmetric and positive definite (i.e., $\mathbf{M}(\boldsymbol{\theta}^{\mathrm{pi}}) = \mathbf{M}^{\mathrm{T}}(\boldsymbol{\theta}^{\mathrm{pi}}) > 0$).

7.2 Potential energy

Assuming the system is rigid, the only source of potential energy is the gravitational potential energy associated with the pendulum. In this paper, we will assume that the sphere is rolling along a flat surface and, therefore, does not contribute any potential energy to the system.

Consider an infinitesimal amount of potential energy

$$dU = -\underset{\rightarrow}{\mathbf{g}} \cdot \underset{\rightarrow}{\mathbf{r}}^{\mathrm{p}}\, dm_{\mathrm{p}}$$

where $\underset{\rightarrow}{\mathbf{g}} := \underset{\rightarrow}{\mathcal{F}}_{\mathrm{i}}^{\mathrm{T}}[0\ 0\ -g]^{\mathrm{T}} = \underset{\rightarrow}{\mathcal{F}}_{\mathrm{i}}^{\mathrm{T}}\mathbf{g}_{\mathrm{i}}$ is the gravitational acceleration vector, and $\underset{\rightarrow}{\mathbf{r}}^{\mathrm{p}}$ is the vectorial position of a mass element dm_{p} as shown in Fig. 4(b). Expanding the infinitesimal potential energy expression gives

$$\begin{aligned} dU &= -\underset{\rightarrow}{\mathcal{F}}_{\mathrm{i}}^{\mathrm{T}}\mathbf{g}_{\mathrm{i}} \cdot \underset{\rightarrow}{\mathcal{F}}_{\mathrm{p}}^{\mathrm{T}}\big(\mathbf{C}_{\mathrm{pi}}\mathbf{r}_{\mathrm{i}}^{\mathrm{pi}} + \mathbf{r}_{\mathrm{p}}^{\mathrm{l}}\big)\, dm_{\mathrm{p}} \\ &= -\big(\mathbf{g}_{\mathrm{i}}^{\mathrm{T}}\mathbf{r}_{\mathrm{i}}^{\mathrm{pi}} + \mathbf{g}_{\mathrm{i}}^{\mathrm{T}}\mathbf{C}_{\mathrm{pi}}^{\mathrm{T}}\mathbf{r}_{\mathrm{p}}^{\mathrm{l}}\big)\, dm_{\mathrm{p}}. \end{aligned}$$

Integrating over the payload/pendulum and noting that $\mathbf{g} \equiv -g\mathbf{z}$, $\mathbf{z}^{\mathrm{T}}\mathbf{r}_{\mathrm{i}}^{\mathrm{pi}} = r$, and $\mathbf{r}_{\mathrm{i}}^{\mathrm{si}} \equiv \mathbf{r}_{\mathrm{i}}^{\mathrm{pi}}$ yields the following

$$\begin{aligned} U &= -m_{\mathrm{p}}\mathbf{g}_{\mathrm{i}}^{\mathrm{T}}\mathbf{r}_{\mathrm{i}}^{\mathrm{pi}} - \mathbf{g}_{\mathrm{i}}^{\mathrm{T}}\mathbf{C}_{\mathrm{pi}}^{\mathrm{T}}\mathbf{c}_{\mathrm{p}} \\ &= gm_{\mathrm{p}}\mathbf{z}^{\mathrm{T}}\mathbf{r}_{\mathrm{i}}^{\mathrm{si}} + g\mathbf{z}^{\mathrm{T}}\mathbf{C}_{\mathrm{pi}}^{\mathrm{T}}\mathbf{c}_{\mathrm{p}}. \end{aligned}$$

7.3 Lagrange's equation

Having developed expressions for the kinetic and potential energy of the unconstrained system, we can define the Lagrangian

$$L = T - U = \frac{1}{2}\dot{\mathbf{q}}^{\mathrm{T}}\bar{\mathbf{S}}^{\mathrm{T}}\mathbf{M}\big(\boldsymbol{\theta}^{\mathrm{pi}}\big)\bar{\mathbf{S}}\dot{\mathbf{q}} - gm_{\mathrm{p}}\mathbf{z}^{\mathrm{T}}\mathbf{r}_{\mathrm{i}}^{\mathrm{si}} - g\mathbf{z}^{\mathrm{T}}\mathbf{C}_{\mathrm{pi}}^{\mathrm{T}}\mathbf{c}_{\mathrm{p}}.$$

We may now employ Lagrange's equation

$$\frac{d}{dt}\left(\frac{\partial L}{\partial \dot{\mathbf{q}}}\right)^{\mathrm{T}} - \frac{\partial L}{\partial \mathbf{q}}^{\mathrm{T}} = \boldsymbol{\Xi}^{\mathrm{T}}\boldsymbol{\lambda} + \mathbf{t}^{\mathrm{f}} + \mathbf{t}^{\mathrm{w}} + \mathbf{t}^{\mathrm{p}} \tag{11}$$

where the $\mathbf{q}$ are the dependent generalized coordinates and $\mathbf{t}^{\mathrm{f}}$, $\mathbf{t}^{\mathrm{w}}$, and $\mathbf{t}^{\mathrm{p}}$ are the generalized forces/torques associated with sphere damping as a result of rolling friction, the wind blowing the sphere, and pendulum damping (also considered energy dissipation/damping due to power generation), respectively. Note that the partial derivative of the Lagrangian with respect to the generalized coordinates, for example, yields a row

$$\frac{\partial L}{\partial \mathbf{q}} = \mathrm{row}\left\{\frac{\partial L}{\partial q_{\mathrm{i}}}\right\}.$$

The matrix $\boldsymbol{\Xi}^{\mathrm{T}}$ is a 9×6 matrix, and $\boldsymbol{\lambda} := [\lambda_1\ \lambda_2\ \lambda_3\ \lambda_4\ \lambda_5\ \lambda_6]^{\mathrm{T}}$ are the Lagrange multipliers associated with the constraints. The reader may quickly realize that $\boldsymbol{\lambda}$ should only be a 5×1 column matrix; there are three constraints associated with the rolling of the sphere, and two constraints associated with the pendulum motion, summing to a total of five constraints. Although it is true, there are only five constraints, by using $\mathbf{C}_{\mathrm{ps}}$ within our definition of $\boldsymbol{\Xi}$ (see (3) and (4)), we have forced $\boldsymbol{\Xi}^{\mathrm{T}}$ to have a 9×6 structure, rather than a 9×5 structure as it naturally should. This, however, is not a problem if one realizes that the fifth row of the matrix $\boldsymbol{\Xi}$, or equivalently the fifth column of $\boldsymbol{\Xi}^{\mathrm{T}}$, is composed of zeros, which renders λ_5 to be of no influence on the equations of motion. The remaining Lagrange multipliers are the ones we are concerned with, but we include all six for the convenience of notation it affords.

Omitting the details for brevity, (11) gives

$$\bar{\mathbf{S}}^{\mathrm{T}}\left(\mathbf{M}\left(\boldsymbol{\theta}^{\mathrm{pi}}\right)\ddot{\mathbf{r}} + \dot{\mathbf{r}}^{\times}\mathbf{M}\left(\boldsymbol{\theta}^{\mathrm{pi}}\right)\dot{\mathbf{r}} + \mathbf{a}\right) = \boldsymbol{\Xi}^{\mathrm{T}}\boldsymbol{\lambda} + \bar{\mathbf{S}}^{\mathrm{T}}\left(\boldsymbol{\tau}^{\mathrm{f}} + \mathbf{f}^{\mathrm{w}} + \boldsymbol{\tau}^{\mathrm{p}}\right) \tag{12}$$

where

$$\mathbf{a} = \begin{bmatrix} -\mathbf{C}_{\mathrm{pi}}^{\mathrm{T}}\boldsymbol{\omega}_{\mathrm{p}}^{\mathrm{pi}\times}\mathbf{c}_{\mathrm{p}}^{\times}\boldsymbol{\omega}_{\mathrm{p}}^{\mathrm{pi}} + \dot{\mathbf{r}}_{\mathrm{i}}^{\mathrm{si}\times}\mathbf{C}_{\mathrm{pi}}^{\mathrm{T}}\mathbf{c}_{\mathrm{p}}^{\times}\boldsymbol{\omega}_{\mathrm{p}}^{\mathrm{pi}} + gm_{\mathrm{p}}\mathbf{z} \\ \mathbf{0} \\ -\boldsymbol{\omega}_{\mathrm{p}}^{\mathrm{pi}\times}\mathbf{c}_{\mathrm{p}}^{\times}\mathbf{C}_{\mathrm{pi}}\dot{\mathbf{r}}_{\mathrm{i}}^{\mathrm{si}} - (\mathbf{C}_{\mathrm{pi}}\mathbf{z})^{\times}\mathbf{c}_{\mathrm{p}}g \end{bmatrix}.$$

Equation (12) could be expanded into nine coupled, non-linear differential equations representing the dynamic motion of the ball rover. We, however, have conveniently been able to express the nine coupled differential equations in matrix form.

8 Expressing the motion equations in terms of the independent generalized coordinates

Having developed the dynamic equations of motion in terms of the dependent generalized coordinates $\dot{\mathbf{r}}$, we will now determine the constrained motion equations in terms of the independent generalized coordinates, $\hat{\boldsymbol{\omega}}$. We will employ the *null space method* [21, 22], which exploits the null space relation of the matrices $\boldsymbol{\Upsilon}$ and $\boldsymbol{\Xi}$ as presented in (7). We are interested in expressing the equations of motion in terms of $\hat{\boldsymbol{\omega}}$ for two reasons: (1) fewer states need to be integrated during simulation, (2) we can avoid calculating the Lagrange multipliers, $\boldsymbol{\lambda}$.

Recall from (7) that $\boldsymbol{\Upsilon}^{\mathrm{T}}\boldsymbol{\Xi}^{\mathrm{T}} = \mathbf{0}$. This relation is the main tool which will allow us to reduce the dynamic equation of motion. By premultiplying (12) by $\boldsymbol{\Upsilon}^{\mathrm{T}}$, the term $\boldsymbol{\Upsilon}^{\mathrm{T}}\boldsymbol{\Xi}^{\mathrm{T}}\boldsymbol{\lambda}$ drops out

$$\boldsymbol{\Upsilon}^{\mathrm{T}}\bar{\mathbf{S}}^{\mathrm{T}}\big(\mathbf{M}(\boldsymbol{\theta}^{\mathrm{pi}})\ddot{\mathbf{r}} + \dot{\mathbf{r}}^{\times}\mathbf{M}(\boldsymbol{\theta}^{\mathrm{pi}})\dot{\mathbf{r}} + \mathbf{a}\big) = \boldsymbol{\Upsilon}^{\mathrm{T}}\bar{\mathbf{S}}^{\mathrm{T}}\big(\boldsymbol{\tau}^{\mathrm{f}} + \mathbf{f}^{\mathrm{w}} + \boldsymbol{\tau}^{\mathrm{p}}\big). \tag{13}$$

The number of equations has been reduced from nine to four. Recall that the physical interpretation of Lagrange multipliers are that they are forces/torques applied such that the constraints are satisfied. In the above, we have avoided the presence of the Lagrange multipliers themselves, but have not avoided their constraining effect. We have merely rearranged the form of the equations such that the algebraic terms associated with the constraints enter into the dynamic equations of constrained motion in a different way.

Before continuing, let us expand and simplify $\boldsymbol{\Upsilon}^{\mathrm{T}}\bar{\mathbf{S}}^{\mathrm{T}}$

$$\begin{aligned}
\boldsymbol{\Upsilon}^{\mathrm{T}}\bar{\mathbf{S}}^{\mathrm{T}} &= \begin{bmatrix} \mathbf{S}_s^{\mathrm{si}\,\mathrm{T}}\mathbf{C}_{\mathrm{si}}\mathbf{z}^{\times}r & \mathbf{1} & \mathbf{S}_s^{\mathrm{si}\,\mathrm{T}}\mathbf{C}_{\mathrm{ps}}^{\mathrm{T}}\mathbf{S}_{\mathrm{p}}^{\mathrm{pi}\,-\mathrm{T}} \\ \mathbf{0} & \mathbf{0} & \mathbf{y}^{\mathrm{T}}\mathbf{S}_{\mathrm{p}}^{\mathrm{pi}\,-\mathrm{T}} \end{bmatrix} \begin{bmatrix} \mathbf{1} & \mathbf{0} & \mathbf{0} \\ \mathbf{0} & \mathbf{S}_{\mathrm{s}}^{\mathrm{si}\,\mathrm{T}} & \mathbf{0} \\ \mathbf{0} & \mathbf{0} & \mathbf{S}_{\mathrm{p}}^{\mathrm{pi}\,\mathrm{T}} \end{bmatrix} \\
&= \begin{bmatrix} \mathbf{S}_{\mathrm{s}}^{\mathrm{si}\,\mathrm{T}} & \mathbf{0} \\ \mathbf{0} & 1 \end{bmatrix} \underbrace{\begin{bmatrix} \mathbf{C}_{\mathrm{si}}\mathbf{z}^{\times}r & \mathbf{1} & \mathbf{C}_{\mathrm{ps}}^{\mathrm{T}} \\ \mathbf{0} & \mathbf{0} & \mathbf{y}^{\mathrm{T}} \end{bmatrix}}_{\boldsymbol{\Delta}} \\
&= \hat{\mathbf{S}}^{\mathrm{T}}\boldsymbol{\Delta}.
\end{aligned} \tag{14}$$

By substitution of (8), (9), and (14) into (13), we have the following

$$\hat{\mathbf{S}}^{\mathrm{T}}\boldsymbol{\Delta}\mathbf{M}(\boldsymbol{\theta}^{\mathrm{pi}})\boldsymbol{\Pi}\dot{\hat{\boldsymbol{\omega}}} + \hat{\mathbf{S}}^{\mathrm{T}}\boldsymbol{\Delta}\big(\mathbf{M}(\boldsymbol{\theta}^{\mathrm{pi}})\dot{\boldsymbol{\Pi}}\hat{\boldsymbol{\omega}} + (\boldsymbol{\Pi}\hat{\boldsymbol{\omega}})^{\times}\mathbf{M}(\boldsymbol{\theta}^{\mathrm{pi}})\boldsymbol{\Pi}\hat{\boldsymbol{\omega}} + \mathbf{a}\big) = \hat{\mathbf{S}}^{\mathrm{T}}\boldsymbol{\Delta}\big(\boldsymbol{\tau}^{\mathrm{f}} + \mathbf{f}^{\mathrm{w}} + \boldsymbol{\tau}^{\mathrm{p}}\big).$$

Each term in the above equation is premultiplied by $\hat{\mathbf{S}}^{\mathrm{T}}$ which is an invertible matrix (provided singularities are avoided). By premultiplying each side by $\hat{\mathbf{S}}^{-\mathrm{T}}$, we can simplify further

$$\boldsymbol{\Delta}\mathbf{M}(\boldsymbol{\theta}^{\mathrm{pi}})\boldsymbol{\Pi}\dot{\hat{\boldsymbol{\omega}}} + \boldsymbol{\Delta}\big(\mathbf{M}(\boldsymbol{\theta}^{\mathrm{pi}})\dot{\boldsymbol{\Pi}}\hat{\boldsymbol{\omega}} + (\boldsymbol{\Pi}\hat{\boldsymbol{\omega}})^{\times}\mathbf{M}(\boldsymbol{\theta}^{\mathrm{pi}})\boldsymbol{\Pi}\hat{\boldsymbol{\omega}} + \mathbf{a}\big) = \boldsymbol{\Delta}\big(\boldsymbol{\tau}^{\mathrm{f}} + \mathbf{f}^{\mathrm{w}} + \boldsymbol{\tau}^{\mathrm{p}}\big). \tag{15}$$

The first term will be written as

$$\hat{\mathbf{M}}(\boldsymbol{\theta}^{\mathrm{si}}, \phi)\dot{\hat{\boldsymbol{\omega}}} := \boldsymbol{\Delta}\mathbf{M}(\boldsymbol{\theta}^{\mathrm{pi}})\boldsymbol{\Pi}\dot{\hat{\boldsymbol{\omega}}}$$

while the second term will be written as

$$\hat{\boldsymbol{\tau}}_{\mathrm{non}} := \boldsymbol{\Delta}\big(\mathbf{M}(\boldsymbol{\theta}^{\mathrm{pi}})\dot{\boldsymbol{\Pi}}\hat{\boldsymbol{\omega}} + (\boldsymbol{\Pi}\hat{\boldsymbol{\omega}})^{\times}\mathbf{M}(\boldsymbol{\theta}^{\mathrm{pi}})\boldsymbol{\Pi}\hat{\boldsymbol{\omega}} + \mathbf{a}\big).$$

The terms associated with damping, wind, and power generation can also be written in a condensed form:

$$\hat{\boldsymbol{\tau}}^{\mathrm{f}} := \boldsymbol{\Delta}\boldsymbol{\tau}^{\mathrm{f}}, \qquad \hat{\boldsymbol{\tau}}^{\mathrm{w}} := \boldsymbol{\Delta}\mathbf{f}^{\mathrm{w}}, \qquad \hat{\boldsymbol{\tau}}^{\mathrm{p}} := \boldsymbol{\Delta}\boldsymbol{\tau}_{\mathrm{p}}.$$

Perhaps the most interesting term is the $\boldsymbol{\Delta}\boldsymbol{\tau}_{\mathrm{p}}$ term, which reduces as follows:

$$\hat{\boldsymbol{\tau}}^{\mathrm{p}} = \boldsymbol{\Delta}\boldsymbol{\tau}_{\mathrm{p}} = \begin{bmatrix} \mathbf{C}_{\mathrm{si}}\mathbf{z}^{\times}r & \mathbf{1} & \mathbf{C}_{\mathrm{ps}}^{\mathrm{T}} \\ \mathbf{0} & \mathbf{0} & \mathbf{y}^{\mathrm{T}} \end{bmatrix} \begin{bmatrix} \mathbf{0} \\ -\mathbf{C}_{\mathrm{ps}}^{\mathrm{T}}\boldsymbol{\tau}_{\mathrm{p}}^{\mathrm{p}} \\ \boldsymbol{\tau}_{\mathrm{p}}^{\mathrm{p}} \end{bmatrix} = \begin{bmatrix} \mathbf{0} \\ \mathbf{y}^{\mathrm{T}}\boldsymbol{\tau}_{\mathrm{p}}^{\mathrm{p}} \end{bmatrix} = \begin{bmatrix} \mathbf{0} \\ -b_{\mathrm{p}}\dot{\phi} \end{bmatrix}. \tag{16}$$

It follows that one may estimate the amount of power generated by employing (16)

$$P = \hat{\boldsymbol{\tau}}^{\mathrm{p}^{\mathrm{T}}} \hat{\boldsymbol{\omega}} = [\mathbf{0} \quad -b_{\mathrm{p}}\dot{\phi}] \begin{bmatrix} \boldsymbol{\omega}_{\mathrm{s}}^{\mathrm{si}} \\ \dot{\phi} \end{bmatrix} = -b_{\mathrm{p}}\dot{\phi}^2.$$

This expression for power is with respect to the sphere-pendulum system, that is power is being 'lost' to the sphere-pendulum system, but power is being 'gained' by the electrical storage system on board the tumbleweed rover.

Combining the above yields the forced, coupled, non-linear differential equations representing the dynamic motion of the ball rover. These motion equations can be written strictly in terms of the independent generalized coordinates

$$\hat{\mathbf{M}}\big(\boldsymbol{\theta}^{\mathrm{si}}, \phi\big)\dot{\hat{\boldsymbol{\omega}}} + \hat{\boldsymbol{\tau}}_{\mathrm{non}} = \hat{\boldsymbol{\tau}}^{\mathrm{f}} + \hat{\boldsymbol{\tau}}^{\mathrm{w}} + \hat{\boldsymbol{\tau}}^{\mathrm{p}}. \tag{17}$$

9 Stability in the sense of Lyapunov

Having completely described the dynamic equations of motion of the system, we now seek to determine if the system is stable. Stability is of concern if our tumbleweed rover is to be a robust platform for exploration. Let us first review the definition of stability in the sense of Lyapunov [23].

Lemma 1 *A dynamical system with states* $\mathbf{x}$ *has a stable equilibrium* $\mathbf{x} = \mathbf{0}$ *if a continuously differentiable function,* $V : D \to \mathbb{R}$, *called a Lyapunov function can be defined such that*

1. $V(\mathbf{0}) = 0$
2. $V(\mathbf{x}) > 0, \forall \mathbf{x} \in D, \mathbf{x} \neq \mathbf{0}$ (*i.e.*, $V(\mathbf{x}(t))$ *is positive-definite in the domain* D)
3. $\dot{V}(\mathbf{x}) \leq 0, \forall \mathbf{x} \in D, \mathbf{x} \neq \mathbf{0}$

Simply stated, for a dynamical system to be stable one needs to show that a Lyapunov function $V(\mathbf{x})$ satisfies conditions 1 through 3 of Lemma 1.

Theorem 1 *Consider the constrained, damped motion of a tumbleweed rover described by* (17) *with* $\hat{\boldsymbol{\tau}}^{\mathrm{w}} = \mathbf{0}$. *The dynamic system with states* $\mathbf{x}^{\mathrm{T}} = [\boldsymbol{\theta}^{\mathrm{si}^{\mathrm{T}}} \ \phi \ \boldsymbol{\omega}_{\mathrm{s}}^{\mathrm{si}^{\mathrm{T}}} \ \dot{\phi}]$ *is stable if* $b_{\mathrm{r}} > 0$, $b_{\mathrm{s}} > 0$ *and* $b_{\mathrm{p}} > 0$.

Proof First note that $\mathbf{x} = \mathbf{0}$ is an equilibrium of (17) when $\hat{\boldsymbol{\tau}}^{\mathrm{w}} = \mathbf{0}$ where $\boldsymbol{\theta}^{\mathrm{si}} = [\gamma \ \beta \ \alpha]^{\mathrm{T}}$. Consider the following Lyapunov function candidate

$$V(\mathbf{x}) := \frac{1}{2}\dot{\mathbf{r}}^{\mathrm{T}}\mathbf{M}\big(\boldsymbol{\theta}^{\mathrm{pi}}\big)\dot{\mathbf{r}} + gm_{\mathrm{p}}r\mathbf{z}^{\mathrm{T}}\mathbf{r}_{\mathrm{i}}^{\mathrm{si}} + g\mathbf{c}_{\mathrm{p}}^{\mathrm{T}}\mathbf{C}_{\mathrm{ps}}\mathbf{C}_{\mathrm{si}}\mathbf{z} - gm_{\mathrm{p}}\left(r - \frac{1}{2}l\right)$$

where $\mathbf{c}_{\mathrm{p}} := -\frac{1}{2}m_{\mathrm{p}}l\mathbf{z}$. The above function is the system Hamiltonian minus a constant related to the potential energy of the system when $\boldsymbol{\theta}^{\mathrm{si}} = \mathbf{0}$, $\phi = 0$. We are writing V in terms of $\dot{\mathbf{r}}$ deliberately. We will define the domain of the Lyapunov function to be

$$D = \left\{ -\frac{\pi}{2} < \gamma, \beta, \alpha, \phi < \frac{\pi}{2}, -\boldsymbol{\omega}_{\mathrm{s}}^{\mathrm{si}'} < \boldsymbol{\omega}_{\mathrm{s}}^{\mathrm{si}} < \boldsymbol{\omega}_{\mathrm{s}}^{\mathrm{si}'}, -\dot{\phi}' < \dot{\phi} < \dot{\phi}' \right\}$$

where $\boldsymbol{\omega}_{\mathrm{s}}^{\mathrm{si}'}$ and $\dot{\phi}'$ are finite, positive angular velocities.

It is straightforward to show that $V(\mathbf{0}) = 0$ and $V(\mathbf{x}) > 0$, $\forall \mathbf{x} \in D$, $\mathbf{x} \neq \mathbf{0}$. Consider the temporal derivative of V

$$\begin{aligned}\dot{V}(\mathbf{x}) &= \dot{\mathbf{r}}^{\mathrm{T}}\mathbf{M}(\boldsymbol{\theta}^{\mathrm{pi}})\ddot{\mathbf{r}} + \frac{1}{2}\dot{\mathbf{r}}^{\mathrm{T}}\dot{\mathbf{M}}(\boldsymbol{\theta}^{\mathrm{pi}})\dot{\mathbf{r}} + \cancelto{0}{gm_{\mathrm{p}}r\mathbf{z}^{\mathrm{T}}\dot{\mathbf{r}}_{\mathrm{i}}^{\mathrm{si}}} + g\mathbf{c}_{\mathrm{p}}^{\mathrm{T}}\dot{\mathbf{C}}_{\mathrm{pi}}\mathbf{z} \\ &= \dot{\mathbf{r}}^{\mathrm{T}}\left(-\dot{\mathbf{r}}^{\times}\mathbf{M}(\boldsymbol{\theta}^{\mathrm{pi}})\dot{\mathbf{r}} - \mathbf{a} + \bar{\mathbf{S}}^{-\mathrm{T}}\boldsymbol{\Xi}\boldsymbol{\lambda} + \boldsymbol{\tau}^{\mathrm{f}} + \boldsymbol{\tau}^{\mathrm{p}}\right) + \frac{1}{2}\dot{\mathbf{r}}^{\mathrm{T}}\dot{\mathbf{M}}(\boldsymbol{\theta}^{\mathrm{pi}})\dot{\mathbf{r}} - g\mathbf{c}_{\mathrm{p}}^{\mathrm{T}}\boldsymbol{\omega}_{\mathrm{p}}^{\mathrm{pi}\times}\mathbf{C}_{\mathrm{pi}}\mathbf{z}. \quad (18)\end{aligned}$$

In the above expansion, we have used (12). After simplification, it can be shown that

$$\dot{V}(\mathbf{x}) = -r^2 b_{\mathrm{r}} \underbrace{\boldsymbol{\omega}_{\mathrm{s}}^{\mathrm{si}\mathrm{T}}\mathbf{C}_{\mathrm{si}}\mathbf{z}^{\times}}_{\mathbf{j}^{\mathrm{T}}} \underbrace{\left(\mathbf{C}_{\mathrm{si}}\mathbf{z}^{\times}\right)^{\mathrm{T}}\boldsymbol{\omega}_{\mathrm{s}}^{\mathrm{si}}}_{\mathbf{j}} - b_{\mathrm{s}} \underbrace{\boldsymbol{\omega}_{\mathrm{s}}^{\mathrm{si}\mathrm{T}}\mathbf{C}_{\mathrm{si}}\mathbf{z}}_{\mathbf{f}^{\mathrm{T}}} \underbrace{(\mathbf{C}_{\mathrm{si}}\mathbf{z})^{\mathrm{T}}\boldsymbol{\omega}_{\mathrm{s}}^{\mathrm{si}}}_{\mathbf{f}} - b_{\mathrm{p}}\dot{\phi}^2 \leq 0.$$

Thus, $\dot{V}$ is negative semi-definite. If, for example, we let $b_{\mathrm{s}} = r^2 b_{\mathrm{r}}$ we can simplify further:

$$\dot{V}(\mathbf{x}) = -b_{\mathrm{s}}\boldsymbol{\omega}_{\mathrm{s}}^{\mathrm{si}\mathrm{T}}\boldsymbol{\omega}_{\mathrm{s}}^{\mathrm{si}} - b_{\mathrm{p}}\dot{\phi}^2 \leq 0$$

where we have used the identity $-\mathbf{z}^{\times}\mathbf{z}^{\times} \equiv \mathbf{1} - \mathbf{z}\mathbf{z}^{\mathrm{T}}$. Therefore, conditions 1 through 3 of Lemma 1 are satisfied, and the system is stable. □

For a system to be asymptotically stable $V(\mathbf{0}) = 0$, $V(\mathbf{x}) > 0$, $\forall \mathbf{x} \in D$, $\mathbf{x} \neq \mathbf{0}$, and $\dot{V}(\mathbf{x}) < 0$, $\forall \mathbf{x} \in D$, $\mathbf{x} \neq \mathbf{0}$. Our Lyapunov function satisfies all these criteria but the last one, that being the requirement that $\dot{V}(\mathbf{x}) < 0$. We have only shown that $\dot{V}(\mathbf{x}) \leq 0$. It should be clear that $\dot{V}$ is negative definite in $\hat{\boldsymbol{\omega}}$, but only negative semi-definite in $\mathbf{x}$, which is why we can only conclude stability, rather than asymptotic stability of the system.

In some situations, asymptotic stability can be concluded by the LaSalle's invariant set theorem. Because our Lyapunov function is continuously differentiable and positive definite in D, we can use a well-known corollary of the more general LaSalle's invariant set theorem. Given $\dot{V}(\mathbf{x}) \leq 0$, $\forall \mathbf{x} \in D$, $\mathbf{x} \neq \mathbf{0}$, define the invariant set as $M = \{\mathbf{x} \in D \mid \dot{V}(\mathbf{x}) = 0\}$. If M contains only $\mathbf{x} = \mathbf{0}$ the system is asymptotically stable. It is insightful for us to investigate our system's invariant set; consider when $\dot{V}(\mathbf{x}) = 0$:

$$\dot{V}(\mathbf{x}) = 0 \quad \Rightarrow \quad \hat{\boldsymbol{\omega}} = \mathbf{0} \quad \Rightarrow \quad \dot{\hat{\boldsymbol{\omega}}} = \mathbf{0}.$$

When $\hat{\boldsymbol{\omega}} = \mathbf{0}$ and $\dot{\hat{\boldsymbol{\omega}}} = \mathbf{0}$ the ball is stationary, and (17) simplifies as follows:

$$\begin{aligned}&\boldsymbol{\Delta}\mathbf{a} = \mathbf{0} \\ &\Leftrightarrow \quad \begin{bmatrix} \mathbf{C}_{\mathrm{si}}\mathbf{z}^{\times}r & \mathbf{1} & \mathbf{C}_{\mathrm{ps}}^{\mathrm{T}} \\ \mathbf{0} & \mathbf{0} & \mathbf{y}^{\mathrm{T}} \end{bmatrix} \begin{bmatrix} gm_{\mathrm{p}}\mathbf{z} \\ \mathbf{0} \\ -(\mathbf{C}_{\mathrm{pi}}\mathbf{z})^{\times}\mathbf{c}_{\mathrm{p}}g \end{bmatrix} = \mathbf{0} \\ &\Leftrightarrow \quad \begin{bmatrix} \frac{1}{2}m_{\mathrm{p}}lg(\mathbf{C}_{\mathrm{si}}\mathbf{z})^{\times}\mathbf{C}_{\mathrm{ps}}^{\mathrm{T}}\mathbf{z} \\ \frac{1}{2}m_{\mathrm{p}}lg\mathbf{y}^{\mathrm{T}}\mathbf{C}_{\mathrm{ps}}(\mathbf{C}_{\mathrm{si}}\mathbf{z})^{\times}\mathbf{C}_{\mathrm{ps}}^{\mathrm{T}}\mathbf{z} \end{bmatrix} = \mathbf{0}.\end{aligned}$$

Using a 3-1-2 Euler angle parameterization [19] for $\mathbf{C}_{\text{si}}$, that is $\mathbf{C}_{\text{si}} = \mathbf{C}_2(\alpha)\mathbf{C}_1(\beta)\mathbf{C}_3(\gamma)$, and knowing $\mathbf{C}_{\text{ps}} = \mathbf{C}_2(\phi)$ the above simplifies further:

$$\begin{bmatrix} \sin\beta\cos\phi \\ \cos\beta(\cos\alpha\sin\phi + \sin\alpha\cos\phi) \\ -\sin\beta\sin\phi \\ \cos\beta(\cos\alpha\sin\phi + \sin\alpha\cos\phi) \end{bmatrix} = \mathbf{0}. \tag{19}$$

If $\gamma = \beta = \alpha = 0$ and $\phi = 0$ (and thus $\mathbf{x} = \mathbf{0}$), the above equality will hold, but the equality will hold for other values of γ, β, α, and ϕ as well. First, γ does not appear anywhere in (19), thus γ may take on any value. When $\gamma \neq 0$, the ball has 'twisted' about the $\vec{\mathbf{i}}_3$-axis. The first element of (19), $\sin\beta\cos\phi$, will be zero if $\beta = 0$, thus ϕ may take on any value. When $\beta = 0$ the central rod is parallel to the ground (that is, the pendulum is hanging straight down). From the second element of (19), given that $\beta = 0$, we have $\cos\alpha\sin\phi + \sin\alpha\cos\phi = \sin(\alpha + \phi) = 0$, which implies $\phi = -\alpha$. When $\phi = -\alpha \neq 0$ the ball has rolled forward or backward. The third and forth elements of (19) are satisfied given $\beta = 0$ and $\phi = -\alpha$. Thus $\gamma \neq 0$, $\beta = 0$, $\alpha \neq 0$, $\phi \neq 0$, and $\hat{\boldsymbol{\omega}} = \mathbf{0}$ satisfies (19). Similarly, $\gamma = 0$, $\beta = 0$, $\alpha \neq 0$, $\phi \neq 0$, and $\hat{\boldsymbol{\omega}} = \mathbf{0}$ satisfies (19) as well.

Clearly, we see that the set invariant set M associated with $\dot{V}(\mathbf{x}) = 0$ does not strictly contain $\mathbf{x} = \mathbf{0}$ and, therefore, the system is not asymptotically stable. However, the solution within the invariant set does match the physical solution we would expect. The ball has stopped moving ($\hat{\boldsymbol{\omega}} = \mathbf{0}$), the central rod is parallel to the ground ($\beta = 0$), the ball may have rolled forward or backward ($\alpha = -\phi \neq 0$), and may also have twisted about $\vec{\mathbf{i}}_3$-axis ($\gamma \neq 0$). Therefore, the solution we have arrived at physically makes sense, and although we are not able to prove asymptotic stability it is clear why it is not possible to do so.

10 Simulation results

Having developed the dynamic equations of motion for the tumbleweed rover, a simple simulation was implemented in order to validate the dynamics model. The physical parameters used to model the system are shown in Table 1. The simulated motion is in terrestrial air, which has a density of $\rho = 1.2$ kg/m^3 at sea level, temperature of 20°C, and 1 atm.

The simulation was executed in MATLAB using the integrator `ode15s`, a solver designed for numerically integrating functions that are 'stiff', such as those with time- and state-dependent mass matrices. To propagate the system's differential equations, both the angular velocity and the Euler angle rates must be integrated. Thus, the full state to be integrated during simulation is

$$\begin{bmatrix} \hat{\boldsymbol{\omega}} \\ \hat{\mathbf{q}} \end{bmatrix}.$$

By rearranging (17), $\dot{\hat{\boldsymbol{\omega}}}$ can be isolated. Similarly, by rearranging $\hat{\boldsymbol{\omega}} = \hat{\mathbf{S}}\dot{\hat{\mathbf{q}}}$, $\dot{\hat{\mathbf{q}}}$ can be isolated:

$$\dot{\hat{\mathbf{q}}} = \begin{bmatrix} \mathbf{S}_{\text{s}}^{\text{si}\,-1} & 0 \\ \mathbf{0} & 1 \end{bmatrix} \hat{\boldsymbol{\omega}}.$$

At each time step, the updated value of $\hat{\boldsymbol{\omega}}$ and $\hat{\mathbf{q}}$ will be available and, therefore, all rotation matrices and angular velocity to Euler angle rate mappings (i.e., $\mathbf{S}_{\text{s}}^{\text{si}\,-1}$) are computable.

Table 1 Physical properties of system

Length of Pendulum	l	0.9 m
Width of Pendulum Rod	w	0.025 m
Height of Payload (Cube)	h	0.1 m
Mass of Pendulum Rod	m_r	5 kg
Mass of Payload (Cube)	m_c	30 kg
First Moment of Mass of Rod	$\mathbf{c}_\mathrm{r}$	$-\frac{1}{2}m_\mathrm{r}l\mathbf{z}$ kg m
Second Moment of Mass of Rod	$\mathbf{J}_\mathrm{r}$	$\mathrm{diag}(\frac{1}{12}m_\mathrm{r}(4l^2+w^2), \frac{1}{12}m_\mathrm{r}(4l^2+w^2), \frac{1}{6}m_\mathrm{r}w^2)$ kg m^2
First Moment of Mass of Payload (Cube)	$\mathbf{c}_\mathrm{r}$	$-\frac{1}{2}m_\mathrm{c}l\mathbf{z}$ kg m
Second Moment of Mass of Payload (Cube)	$\mathbf{J}_\mathrm{c}$	$\mathrm{diag}(\frac{1}{6}m_\mathrm{c}(h^2+6l^2), \frac{1}{6}m_\mathrm{c}(h^2+6l^2), \frac{1}{6}m_\mathrm{c}w^2)$ kg m^2
First Moment of Mass of Pendulum	$\mathbf{c}_\mathrm{p}$	$\mathbf{c}_\mathrm{p} = \mathbf{c}_\mathrm{r} + \mathbf{c}_\mathrm{c}$
Second Moment of Mass of Rod	$\mathbf{J}_\mathrm{p}$	$\mathbf{J}_\mathrm{p} = \mathbf{J}_\mathrm{r} + \mathbf{J}_\mathrm{c}$
Pendulum Damping Coefficient	b_p	1.5 $\frac{\mathrm{kg\,m^2}}{\mathrm{s}}$
Radius of Sphere	r	1 m
Mass of Sphere	m_s	5 kg
Second Moment of Mass of Sphere	$\mathbf{J}_\mathrm{s}$	$\frac{2}{3}m_\mathrm{s}r^2\mathbf{1}$ kg m^2
Sphere Damping Coefficient	$b_\mathrm{r}, b_\mathrm{s}$	$b_\mathrm{r} = 3.5$ $\frac{\mathrm{kg\,m^2}}{\mathrm{s}}$, $b_\mathrm{s} = r^2 b_\mathrm{r}$

Similarly, once $\boldsymbol{\omega}_\mathrm{s}^\mathrm{si}$ is known, (1) can be used to determine the translational velocity of the system over time, which can be integrated to yield the position of the ball over time.

First, we will show the simulation results for the nominal case of wind blowing down the $\vec{\mathbf{i}}_\mathrm{l}$-axis at a velocity of $v_\mathrm{ave} = 30$ km/h. The wind velocity will be governed by $v(t) = v_\mathrm{ave}(1 - e^{t/2})$; the wind velocity will initially be zero and increase to the average wind velocity over a relatively short period of time. Recall $\boldsymbol{\theta}^\mathrm{si} = [\gamma\ \beta\ \alpha]^\mathrm{T}$; the rover will start with all Euler angles initially zero (including ϕ) and an initial angular velocity of $\boldsymbol{\omega}_\mathrm{s}^\mathrm{si} = [0\ 5\ 0]^\mathrm{T}$ rad/s, $\dot{\phi} = 0$ rad/s. Figures 5 and 6 show the angular velocity and the Euler angles as functions of time. Figures 7 and 8 show the translational velocity and position of the rover as it rolls.

It is interesting to see that for approximately the first 20 s or so of the simulation, the pendulum is 'wobbling' forward and aft, thus causing the sphere to wobble forward and aft as well. Eventually enough energy is damped out of the system so that the ball finally rolls smoothly along the $\vec{\mathbf{i}}_\mathrm{l}$-axis.

Next, we will present results for initially non-zero Euler angles (i.e., non-zero attitude). The initial angular velocity will be $\boldsymbol{\omega}_\mathrm{s}^\mathrm{si} = [0\ 2\ 0]^\mathrm{T}$ rad/s, $\dot{\phi} = -1$ rad/s, and the Euler angles will be $\boldsymbol{\theta}^\mathrm{si} = [\gamma\ \beta\ \alpha]^\mathrm{T} = [5^\circ\ 10^\circ\ 0]^\mathrm{T}$ and $\phi = -10^\circ$. Shown in Figs. 9 and 10 are the angular velocity and the Euler angles as a function of time. In Figs. 11 and 12 are the translational velocity and position of the rover as it rolls. In Fig. 13 is the wind force as a function of time, showing how the wind force changes as the ball speeds up.[4]

In Figs. 9 and 10, it can be seen that the ball is initially oscillating in a 'side-to-side' manner about β and a 'twist' manner about γ due to the initial non-zero angle β. After 10 s to 15 s the oscillation dampens, and the ball rolls smoothly down the $\vec{\mathbf{i}}_\mathrm{l}$-axis. Due to the non-zero initial conditions, the system acquires a velocity in the $\vec{\mathbf{i}}_2$ direction which is eventually

[4]Recall that wind force is a function of the relative velocity between the wind and the ball.

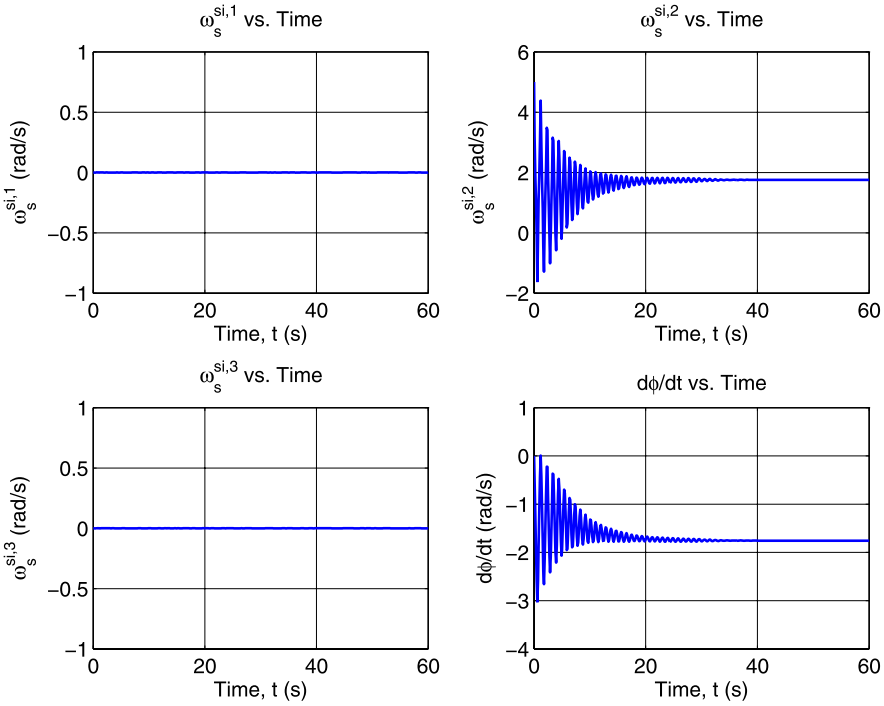

Fig. 5 Angular velocity, $\boldsymbol{\omega}_s^{si}$ and $\dot{\phi}$

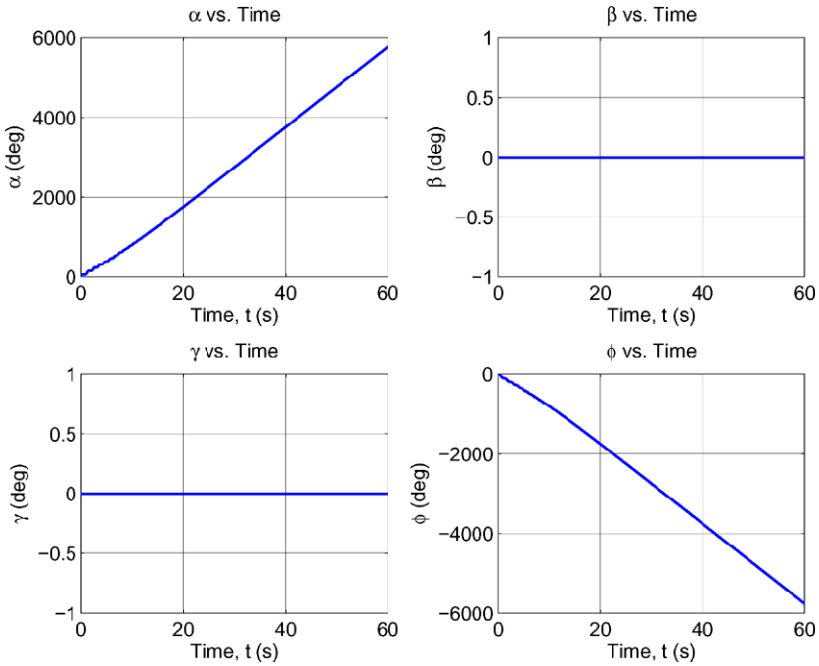

Fig. 6 Euler angles, α, β, γ and ϕ

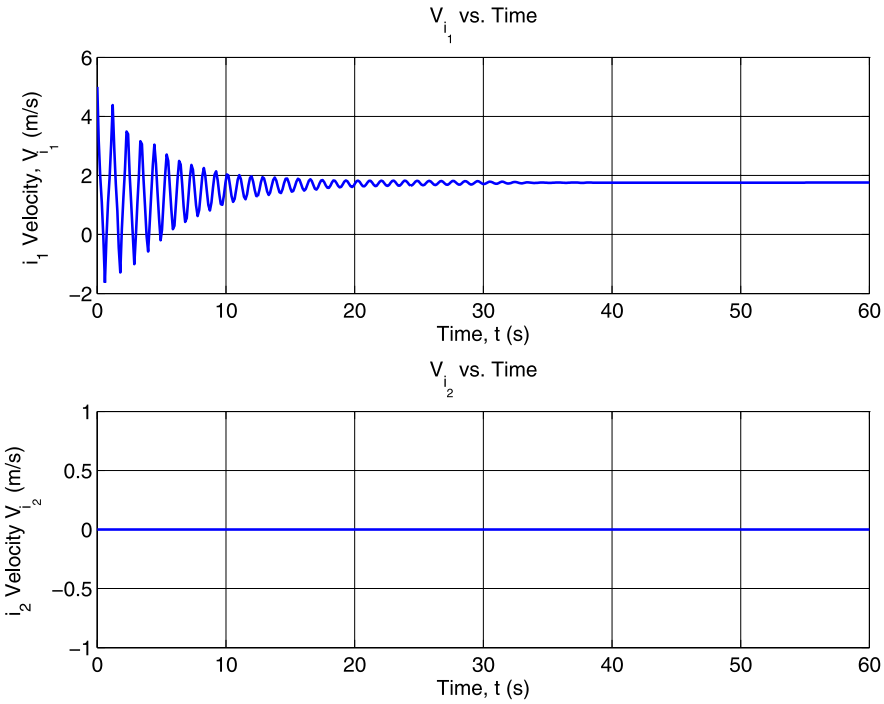

Fig. 7 Translational velocity in $\underrightarrow{\mathbf{i}}_1$ and $\underrightarrow{\mathbf{i}}_2$

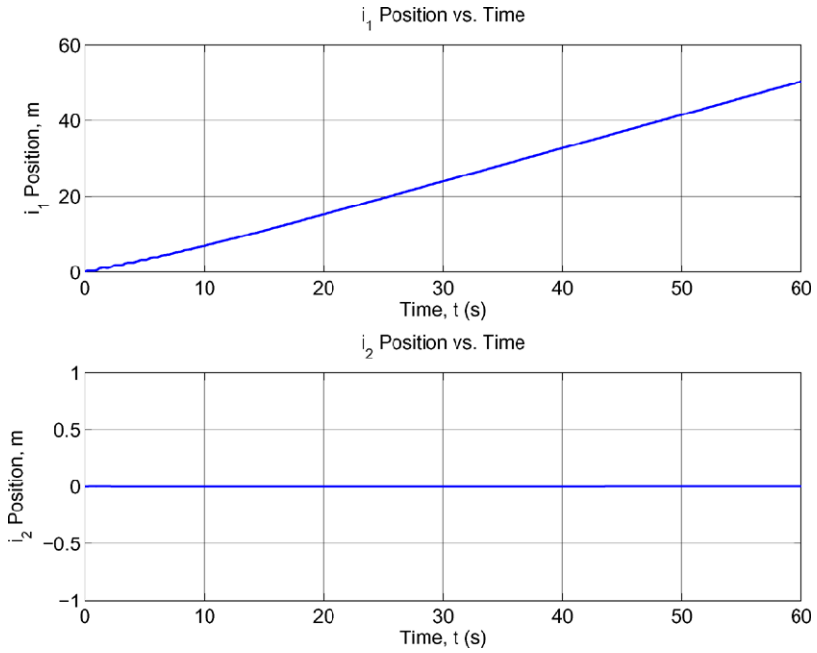

Fig. 8 Translational position in $\underrightarrow{\mathbf{i}}_1$ and $\underrightarrow{\mathbf{i}}_2$

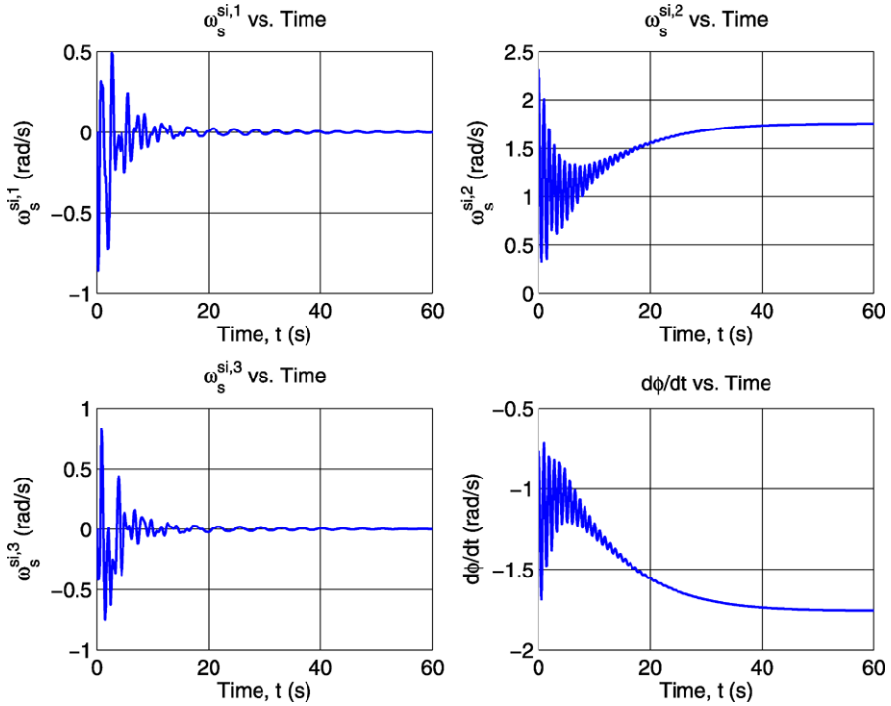

Fig. 9 Angular velocity, $\boldsymbol{\omega}_s^{si}$ and $\dot{\phi}$ (nonzero Euler angles at $t = 0$)

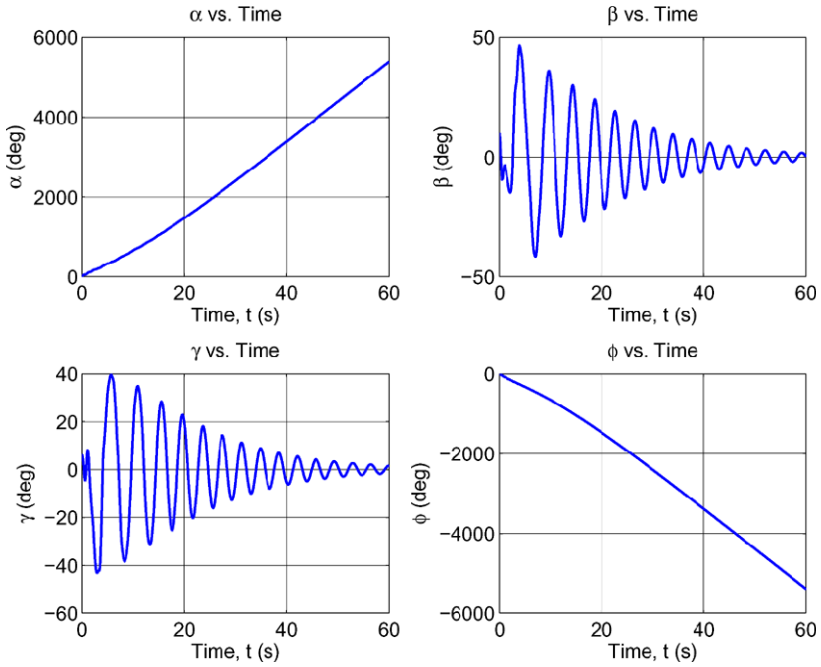

Fig. 10 Euler angles, α, β γ and ϕ (non-zero Euler angles at $t = 0$)

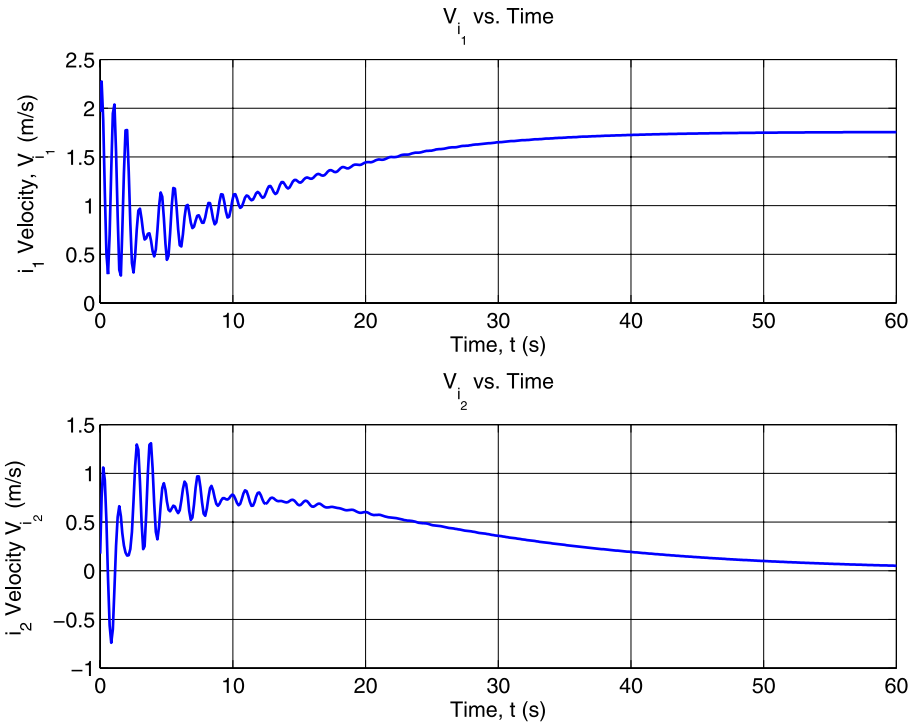

Fig. 11 Translational velocity in $\vec{\mathbf{i}}_1$ and $\vec{\mathbf{i}}_2$ (non-zero Euler angles at $t = 0$)

damped out as shown in Fig. 11. This leads to an translational offset in the $\vec{\mathbf{i}}_2$ direction as shown in Fig. 12, as well as a small force as shown in Fig. 13, which eventually subsides as the velocity in $\vec{\mathbf{i}}_2$ decreases to zero. This simulation shows that our design is able to roll stably downwind (with the pendulum laterally fixed) while generating power.

11 Conclusions and future work

We have presented a new concept for a tumbleweed rover that incorporates an internal pendulum-generator system, primarily as a means to generate electrical power. The focus of the paper was to present a first-principles development of the dynamics of this complex system including such effects as the internal pendulum dynamics, resistance (damping) provided by the electrical generators, external wind force, and rolling constraints between the sphere and the ground. It also specialized the model to the case of the pendulum being laterally fixed and it was shown both theoretically and through simulations that the design is stable.

The fact that this tumbleweed is stable is perhaps not surprising for the case of rolling downwind. The reason is that the pendulum swings backwards, thereby shifting the center of mass aft. This induces a situation similar to a 'weather helm' in sailing vessels. With the center of mass aft, the wind always helps point the tumbleweed downwind. Still, the model is very useful as it allows us to simulate motion for a variety of parameter values and wind

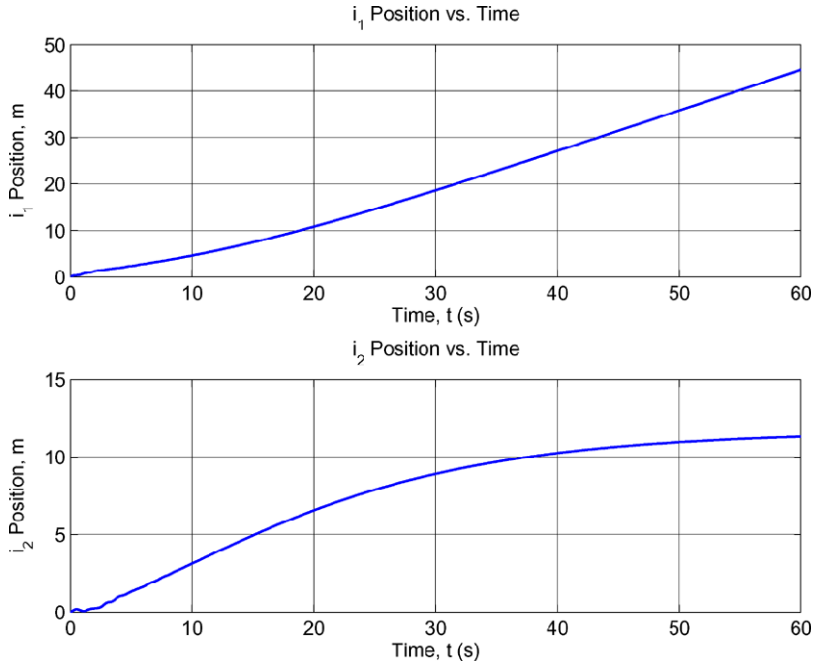

Fig. 12 Translational position in $\underrightarrow{\mathbf{i}}_1$ and $\underrightarrow{\mathbf{i}}_2$ (non-zero Euler angles at $t = 0$)

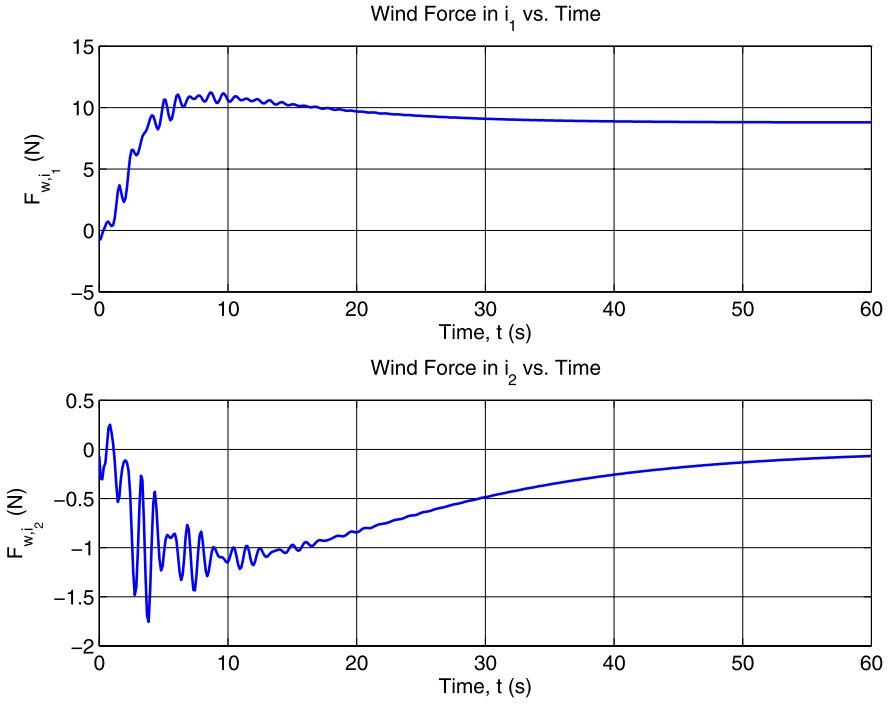

Fig. 13 Wind force in $\underrightarrow{\mathbf{i}}_1$ and $\underrightarrow{\mathbf{i}}_2$ (non-zero Euler angles at $t = 0$)

conditions. This is an important stepping stone on the path to prototyping the pendulum tumbleweed design, which is our next logical step.

Feedback control of our platform is also an area of future investigation. By regulating the amount of power removed from the system, it should be possible to control the speed of the rover. Actively steering the rover in the presence of wind is also of interest. This could dovetail nicely with the fact that the pendulum provides a stable platform that could be used to house cameras and other sensors that look ahead to detect hazards.

Although the model does a good job, primarily of helping us understand the complex attitude dynamics of the tumbleweed, there are certainly several effects that we have deliberately neglected including asphericity of the ball, bouncing, collisions with obstacles, and ground effects (i.e., the rover is rolling in a fluid boundary layer). As part of our future work, we hope to extend our model to incorporate some of these effects, but others will be investigated through experiments.

References

1. Maimone, M.: Surface navigation and mobility intelligence on the mars exploration rovers. In: Howard, A., Tunstel, E. (eds.) Intelligence for Space Robotics, pp. 45–70. TSI Press, San Antonio (2006). Chap. 3
2. Behar, A., Matthews, J., Carsey, F., Jones, J.: NASA/JPL tumbleweed polar rover (1003) (2004)
3. Jones, J.: Inflatable robotics for planetary applications. In: Proceedings of the International Symposium on Artificial Intelligence and Robotics and Automation in Space (iSAIRAS), St. Hubert, Quebec, Canada (2001)
4. Antol, J., Calhoun, P., Flick, J., Hajos, G., Kolacinski, R., Minton, D., Owens, R., Parker, J.: Low cost Mars surface exploration: the Mars tumbleweed. Tech. Rep. TM-2003-212411, NASA (2003)
5. Hoeg, T., Southard, L., Boxerbaum, A., Reis, L., Antol, J., Heldmann, J., Quinn, R.: Tumbleweed rover science mission to Dao Vallis. In: Proceedings of the AIAA Aerospace Sciences Meeting and Exhibit, 2006-70, Reno, Nevada (2006)
6. Southard, L., Hoeg, T., Palmer, D., Antol, J., Roger Quinn, R.K.: Exploring Mars using a group of tumbleweed rovers. In: Proceedings IEEE International Conference on Robotics and Automation (ICRA), pp. 775–780, Roma, Italy (2007)
7. Antol, J., Woodard, S., Hajos, G.: Using wind driven tumbleweed rovers to explore martian gully features. In: Proceedings of the AIAA Aerospace Sciences Meeting and Exhibit, 2005-245, Reno, Nevada (2005)
8. Lorenz, R., Jones, J., Wu, J.: Mars magnetometry from a tumbleweed rover. In: IEEEAC (1054) (2003)
9. Matthews, J.: Development of the tumbleweed rover. Tech. Rep., Jet Propulsion Laboratory (2003)
10. Lorenz, R., Behar, A., Nicaise, F., Jonsson, J., Myers, M.: Field testing and dynamic model development for a Mars tumbleweed rover. In: Proceedings of the International Planetary Probe Workshop, Pasadena, CA (2006)
11. Kolacinski, R., Quinn, R.: Design of a biologically inspired martian rover based upon the Russian thistle (salsola tragus). In: Proceedings of the Dynamics and Control of Space Structures Symposium (DCSSS04), Italy (2004)
12. Antol, J., Harris, S., Hajos, G., Strickland, C.: Wind tunnel tests of evolved Mars tumbleweed concepts. In: Proceedings of the AIAA Aerospace Sciences Meeting and Exhibit, 2006-69, Reno, Nevada (2006)
13. Antol, J., Chattin, R., Copeland, B., Krizan, S.: The NASA Langley mars tumbleweed rover prototype. In: Proceedings of the AIAA Aerospace Sciences Meeting and Exhibit, 2006-64, Reno, Nevada (2006)
14. Claycomb, J., DeJarnette, F., Mazzoleni, A.: Development and construction of a prototype Mars tumbleweed rover. In: Proceedings of the AIAA Aerospace Sciences Meeting and Exhibit, 2006-66, Reno, Nevada (2006)
15. DeJarnette, F., Casper, K., Maxwell, B., Schwarz, J., Sebastian, T., Engler, W., Hanrahan, H., Lam, N.: Deployment devices and solar power for Mars tumbleweed rovers. In: Proceedings of the AIAA Aerospace Sciences Meeting and Exhibit, 2005-246, Reno, Nevada (2005)
16. Suomela, J., Ylikorpi, T.: Ball-shaped robots: an historical overview and recent developments at TKK. In: Corke, P., Sukkarieh, S. (eds.) Field and Services Robotics, STAR, pp. 343–354. Springer, Berlin (2006)

17. Wilson, J., Hartl, A., Mazzoleni, A., DeJarnette, F.: Dynamics modeling of a Mars tumbleweed rover. In: Proceedings of the AIAA Aerospace Sciences Meeting and Exhibit, 2006-71, Reno, Nevada (2006)
18. Basic, G.: Tumbleweed rover technology developments: Overview of prototype designs, field tests, aerodynamics and dynamics analysis. Tech. Rep., University of Toronto Institute for Aerospace Studies (2008)
19. Hughes, P.C.: Spacecraft Attitude Dynamics, 2nd edn. Dover, Mineola (2004)
20. White, F.M.: Fluid Mechanics, 5th edn. McGraw-Hill, New York (2003)
21. Damaren, C.J.: On the dynamics and control of flexible multibody systems with closed loops. Int. J. Robot. Res. **19**(3), 238–253 (2000)
22. Campion, G., d'Andrea Novel, B., Bastin, G.: Controllability and state feedback stabilizability of non holonomic mechanical systems. In: Advanced Robot Control: Proceedings of the International Workshop on Nonlinear and Adaptive Control: Issues in Robotics. Grenoble, France (1990)
23. Marquez, H.: Nonlinear Control Systems. Wiley, Hoboken (2003)